UNIVERSITE JOSEPH KI-ZERBO

ECOLE DOCTORALE INFORMATIQUE
ET CHANGEMENTS CLIMATIQUES

BURKINA FASO

Unité-Progrès-Justice

MASTER RESEARCH PROGRAM

SPECIALITY: INFORMATICS FOR CLIMATE CHANGE (ICC)

MASTER THESIS

Subject:

POTENTIAL IMPACT OF SOLAR GEOENGINEERING ON RENEWABLE ENERGY OVER WEST AFRICA

Presented on July 15, 2022 by:

Kefo Apa Habiba Christiane COULIBALY

Jury members

President: **Prof Tizane DAHO**

Reviewer: **Dr Bruno KORGO**

Supervisor: **Dr Ousmane COULIBALY**

Major Supervisor

Dr Ousmane COULIBALY

Co-Supervisor

Dr Windmanagda SAWADOGO

Academic year 2021-2022

Dedication

Glory to God, the Almighty, creator of heaven and earth, the visible and invisible world, for the grace to produce this document.

To my parents, source of life, love, and affection, I give thanks for the upbringing that made me what I am today and for all their sacrifices. May God grant them health and long life.

Acknowledgements

These two years have been so rich in encounters that I would like to express my sincere gratitude to them. This project would not have been possible without the support and help of many people.

First and foremost, I would like to thank the donors BMBF and WASCAL for the opportunity of this scholarship, which allowed me to carry out this work.

My thanks go to the members of the administration on the "Ecole doctorale Informatique et Changement Climatique" (ED-ICC) led by the director Professor Pierre ZOUNGRANA. I am particularly grateful to the Deputy Director of ED-ICC, Dr Ousmane COULIBALY, who is my main supervisor, for his availability and attention. I also thank the scientific coordinator, Dr Benewindé ZOUNGRANA, for his open-mindedness and advice which allowed us to structure our research well. My thanks also go to the lecturers of the programme ED-ICC for the quality of the training.

I am very indebted to my co-supervisor Dr Windmanagda SAWADOGO for his advice and constant supervision and for providing the necessary information about the project and also for his support in the carrying out of the project.

I am also grateful to Dr Romaric ODOULAMI for his help and willingness to share his vast knowledge to help us understand this project.

My thanks also go to my classmates in the ED-ICC programme for their support and brotherhood during this study.

To my family and all those whose names cannot be mentioned and who have supported me, I would like to express my deep gratitude here.

Abstract

Renewable energy resources can be sensitive to future climate change. Geoengineering is suggested as a potential way to reduce the climate impacts of global warming. Here, we assess the potential impact of a solar geoengineering approach on renewable energy resources, such as solar and wind energy over West Africa. This research is one of the first studies in Africa to investigate the potential impact of solar geoengineering activities on renewable energy using state-of-the-art GeoMIP climate models to contributing to the current research portfolio on the future of renewable energy. Three CMIP6 (Coupled Model Intercomparison Project Phase 6) under climate change scenarios SSP2-4.5 and SSP5-8.5 were used in this study. We also used the corresponding simulations from GeoMIP6 (Geoengineering Model Intercomparison Project Phase 6), in particular the G6sulfur experiment, where sulphur particles are introduced into the upper atmosphere. The projections focus on the far future (2070-2099). The performance of the different models and their ensemble mean (Rmean) is first evaluated using the ERA5 reanalysis data for the period (1985-2014). The simulations with their Rmean reproduce well the pattern of observation of different variables with notable biases. The results show that G6sulfur tends to reduce temperature and wind speed but increase solar irradiance over West Africa. In addition, the solar PV potential increases and the wind power density decreases with G6sulfur experiment compared to the SSP5-8.5 scenarios. There are still differences in the projected changes in renewable energy and its different drivers, such as in the case of West Africa, suggesting that further refinement of the model is needed before attempting to draw conclusions on potential changes through geoengineering simulations.

Key words: Climate change; Geoengineering; CMIP6; G6sulfur; Renewable energy; West Africa.

Résumé

Les ressources énergétiques renouvelables peuvent être sensibles aux changements climatiques futurs. La géo-ingénierie a été proposée pour lutter contre le changement climatique. Cette solution vise à réduire le réchauffement de la planète. Cette étude porte sur l'évaluation du potentiel impact de la géo-ingénierie sur les ressources énergétiques renouvelables, telles que l'énergie solaire et éolienne, en Afrique de l'Ouest. Cette recherche est l'une des premières études en Afrique à examiner les conséquences des activités de géo-ingénierie sur les énergies renouvelables en utilisant des modèles climatiques GeoMIP afin de contribuer au portefeuille de recherche actuel sur l'avenir des énergies renouvelables. Trois modèles CMIP6 (Coupled Model Intercomparison Project Phase 6) sous les scénarios de changement climatique SSP2-4.5 et SSP5-8.5 ont été utilisés dans cette étude. Nous avons également utilisé les simulations correspondantes de GeoMIP6 (Geoengineering Model Intercomparison Project Phase 6), en particulier l'expérience G6sulfur, où des particules de soufre sont introduites dans l'atmosphère. Les projections sont focalisées sur le futur lointain (2070-2099). La performance des différents modèles et de leur moyenne d'ensemble (Rmean) est d'abord évaluée en utilisant les données de réanalyse ERA5 pour la période allant de 1985 à 2014. Les simulations avec leur Rmean reproduisent bien le modèle d'observation des différentes variables avec des biais notables. Les résultats montrent que le G6sulfur tend à réduire la température et la vitesse du vent mais à augmenter l'irradiance solaire sur l'Afrique de l'Ouest. En outre, le potentiel solaire photovoltaïque augmente et la densité de puissance éolienne diminue avec l'expérience G6sulfur par rapport aux scénarios SSP5-8.5. Il existe encore des différences dans les changements projetés en matière d'énergie renouvelable et ses différents moteurs, comme dans le cas de l'Afrique de l'Ouest, ce qui suggère que le modèle doit être affiné davantage avant de tenter de tirer des conclusions sur les changements potentiels par des simulations de géo-ingénierie.

Mots clés : Changement climatique ; géo-ingénierie ; CMIP6 ; G6sulfur ; Energie renouvelable ; Afrique de l'Ouest.

Acronyms and abbreviations

CDR: Carbon Dioxide Removal

CMIP6: Coupled Model Intercomparison Project phase 6

CO_2: Carbon dioxide

GCM: Global Climate Model

GeoMIP6: Geoengineering Model Intercomparison Project phase 6

GHG: Greenhouse Gas

IPCC: Intergovernmental Panel for Climate Change

IRENA: International Renewable Energy Agency

PVP: Photovoltaic Power Potential

SAI: Stratospheric sulphate Aerosol Injection

SO_2: Sulfur dioxide

SRM: Solar Radiation Management

WPD: Wind Power Density

List of tables

List of figures

Introduction

Energy is essential for our society to ensure high quality of life and to run most socio-economic activities. However, More than 80% of energy production comes from fossil fuels (Yu et al., 2008), which release carbon dioxide (CO_2) into the atmosphere. The increase in the atmospheric emissions of CO_2 contributes to the increase in global average temperature inducing global warming. Working Group I of the Intergovernmental Panel on Climate Change (IPCC, 2021) in the Sixth Assessment Report showed that global surface temperature has been rising faster. The rapid rise in global average temperature has scientists on the alert advising policy makers to limit our CO_2 emissions. It is likely that we will reach or exceed 1.5 degrees Celsius (2.7 degrees F) of warming within the next two decades. To avoid that, renewable energy is one of the alternatives solutions to reduce our carbon footprint.

Renewable energies are energy sources that are continuously replenished by nature (Ellabban et al., 2014). Their technologies offer an excellent opportunity to reduce greenhouse gas (GHG) emissions and thus, global warming by replacing conventional energy sources. Moreover, renewable energy promises clean, abundant energy derived from self-renewing resources such as the sun, wind, earth, and plants (Panwar et al., 2011). The potential of renewable energy resources is enormous, as they can in principle exponentially exceed global energy demand. These types of resources will therefore have an important share in the future global energy portfolio, much of which is currently focused on renewable energy (Ellabban et al., 2014). African countries have high renewable energy potential, which is particularly evident in Africa, where solar, wind, hydro, geothermal and biomass resources are abundant. Indeed, they play an important role in electrification and are considered the energy of the future.

The use of renewable energy sources such as solar and wind energy has increased since the last decades in Africa, especially in West Africa for electricity generation. Many West African countries are in the process of expanding solar and wind energy in their electricity. However, a study by (Sawadogo et al., 2020) on West Africa showed that solar energy based on photovoltaic technology and that efficiency decreases when the global average temperature increases. In addition, (Sawadogo et al., 2019) projected a slight increase in wind power density over the West Africa regions when global temperature increases. These studies show that global warming has an

impact on renewable energy sources in West Africa Nonetheless, many scenarios have been considered to keep the average temperature increase below +2 °C. Given society's failure to take concerted action to address global warming, and despite the Paris Agreement which aims to keep the increase in average global temperature well below 2°C above pre-industrial levels, climate scientists like (Turner et al., 2010) and (Crutzen, 2006), suggest that society should consider geoengineering solutions to combat global warming (Robock, 2015).

The term « geoengineering » refers to large-scale efforts to reduce the impacts of climate change caused by GHGs already released into the atmosphere. Geoengineering is not a technology that is ready for use in the immediate future. It is, however, a technology that could be useful at some point in the future when it might be needed. But its implementation requires a full understanding of its potential benefits and side effects on the environmental and society.

However, any benefits come with novel risks and significant uncertainty. For example, previous studies have shown that geoengineering activities could negatively affect natural ecosystems (Russell et al., 2012), regional climate extremes (Pinto et al., 2020), West African summer monsoon precipitation (Da-Allada et al., 2020), agriculture in Africa (ETC Group, 2014), and affect the potential of all direct and indirect solar renewable energy, including biomass, hydro, wind, as well as photovoltaic and solar thermal energy conversion (Moriarty & Honnery, 2013).
To date, there is a little study on the impact of solar geoengineering on renewable energy over West Africa. This study will help scientists and policy makers better understand the limitations, uncertainties, and risks of geoengineering.

a. Study objectives

a.1. Main objective

This study aims is to investigate the impact of solar geoengineering through sulfate stratospheric injection on solar and wind energy potential in West Africa.

a.2. Specific objectives

To achieve this aim, three specific objectives are defined:

- to evaluate the CMIP6 models in the simulation of solar and wind energy potential and their various drivers in the current climate over West Africa;

- to assess the impact of the solar geoengineering on photovoltaic power potential (PVP) in West Africa; and,
- to assess the impact of solar geoengineering on wind power density (WPD) in West Africa.

b. Research questions

b.1. Main research question

The main research question behind this study is how solar geoengineering could influence solar and wind energy potential in West Africa.

b.2. Specific research questions

The specific questions are defined as follows:

- How well the CMIP6 models reproduce the PVP and WPD and their various drivers in the current climate over West Africa?
- What is the impact of solar geoengineering on PVP in West Africa?
- What is the impact of solar geoengineering on WPD in West Africa?

c. Research hypothesis

c.1. Main research hypothesis

For the main research hypothesis, we assume that solar geoengineering could decrease the potential of solar and wind energy in West Africa.

c.2. Specific research hypothesis

- CMIP6 models reproduce well the current climate of PVP and WPD and their different drivers in West Africa.
- Solar geoengineering could reduce the PVP in West Africa.
- Solar geoengineering could have negative impact on the WPD in West Africa.

This master's thesis consists of three chapters. The first part focuses on the background of the study, the problem statement and justification, the objectives of the study, the research questions and, the research hypothesis. Then, chapter 1 presents the literature review. It includes the definition, the different methods, some background information on geoengineering and provide a summary of previous work on the impact of solar geoengineering. Chapter 2 describes the study area, the data and the methodology used in this study. Chapter 3 mainly focuses on the main findings and discussions. Finally, the last part concludes the thesis and recommendations.

Chapter 1: LITERATURE REVIEW

This chapter describes geoengineering and its different methods. It also explains the different types of GeoMIP available and provides a summary of previous studies based on geoengineering.

1.1.Background

Geoengineering is an intentional large-scale manipulation of the environment to partially offset some of the impacts of climate change (Keith, 2000). For an intervention to be considered geoengineering, environmental change must be the primary goal, not just a side effect, and the intent and impact of the manipulation must be at large-scale. Two basic characteristics will serve as markers for geoengineering:

1. Scope: the impact of the manipulation of geoengineering must be continental or global,
2. Intent: the manipulation of geoengineering must have an intentional desire to change the atmospheric conditions to solve a problem.

The first use of the term geoengineering as defined above was described by Marchetti in the early 1970s to describe the reduction of climate impacts caused by fossil fuel combustion by injecting carbon dioxide into the deep ocean (Keith, 2000). Climate geoengineering is proposed as a way to address carbon dioxide-related climate problems. **Figure 1** shows a diagram of a climate problem for which mitigation, geoengineering, or adaptation is the response strategy. In this diagram, geoengineering is any manipulation of the climate system to alter its response to anthropogenic forcing.

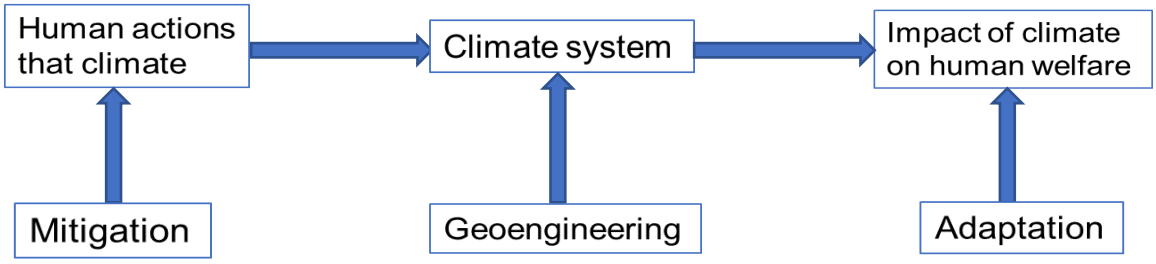

Figure 1: Three-part schema of the climate problem. Source: (Keith, 2000)

1.2. Geoengineering's methods

Geoengineering is usually divided into two broad categories:

The first is carbon geoengineering, often called carbon dioxide removal (CDR). The other is solar geoengineering, often called solar radiation management (SRM), albedo modification, or sunlight reflection.

1.2.1. Carbon Dioxide Removal (CDR)

Carbon geoengineering aims to remove carbon dioxide from the atmosphere and thus, address the root cause of climate change, namely the accumulation of carbon dioxide - and other greenhouse gases - in the atmosphere. In the chain between emissions, concentrations, temperatures and impacts, it breaks the link between emissions and concentrations.

Human activities perturbate the natural carbon cycle by releasing excessive amount of CO_2 into the atmosphere through emission from fossil-fuels burning and land-use change. CDR approaches aim to remove excess CO_2 directly from the atmosphere and store the carbon in the land biosphere, ocean, or deep geological reservoirs (**Figure 2**).

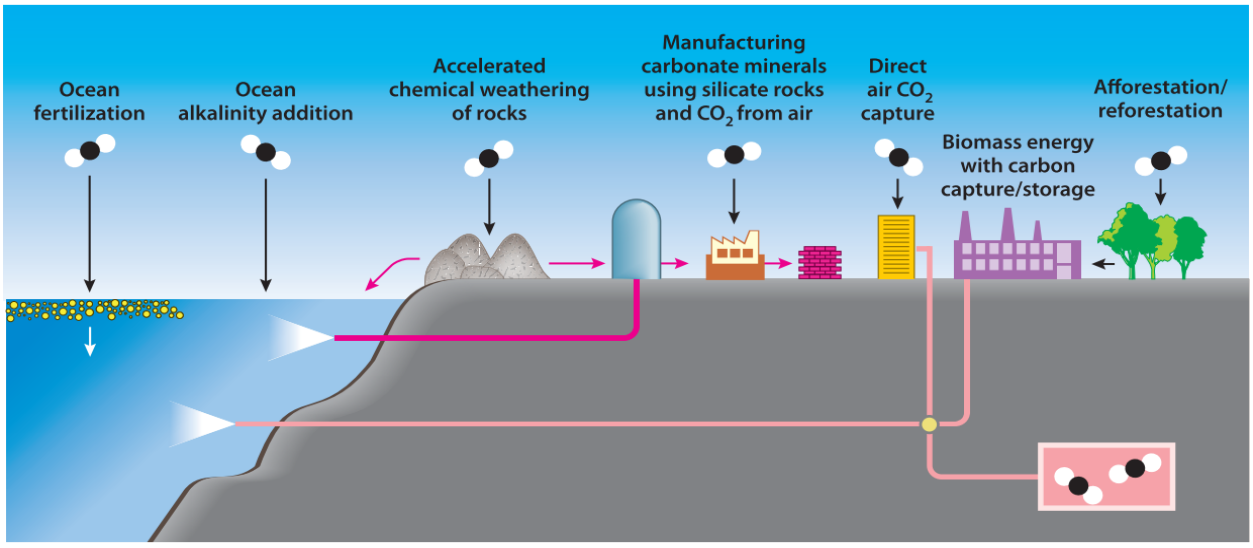

Figure 2 : Diagram illustrating carbon dioxide removal approaches. Source:(Caldeira et al., 2013)

1.2.2. Solar Radiation Management (SRM)

Solar geoengineering approaches aim to offset the influence of global warming by reducing the amount of sunlight absorbed by the Earth. Unlike carbon geoengineering, solar geoengineering is not about the root cause of climate change. Instead, it aims to break the link between CO_2 concentrations and temperatures, thereby reducing some of the climate damage.

Proposed solar geoengineering technologies (**Figure 3**) include:

- Marine cloud brightening

Marine cloud brightening would aim to brighten marine clouds to reflect more sunlight back into space.

- Thinning cirrus cloud

They would seek to reduce thin cirrus clouds at high-altitude to allow the Earth to emit more longwave radiation into space.

- Space-based techniques

Space technologies would work to reflect a small amount of sunlight away from Earth by positioning solar shields in space.

- Stratospheric aerosol scattering

Stratospheric aerosol scattering would introduce tiny reflective particles, such as sulphate aerosols or calcium carbonate, into the upper atmosphere, where they could scatter a small fraction of sunlight back into space.

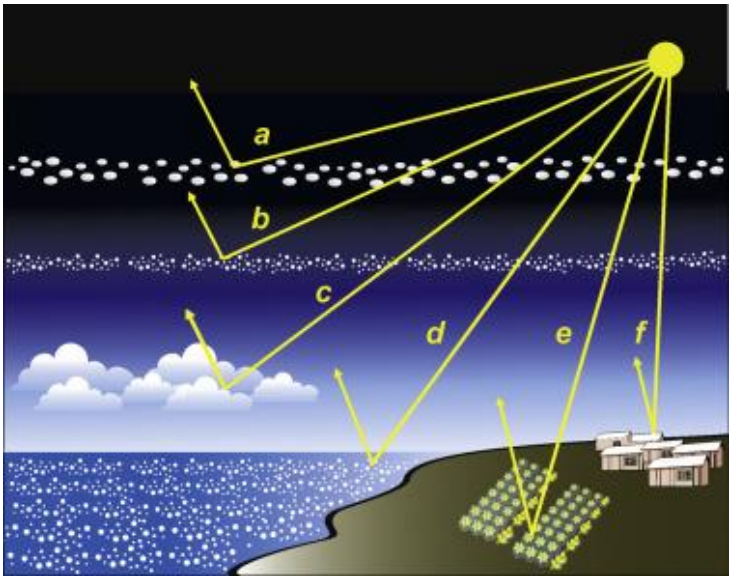

Figure 3 : Diagram illustrating solar geoengineering approaches, a-using space mirrors, b-injecting aerosols into the stratosphere, c-brightening marine clouds, d-increasing the reflectivity of the ocean surface, e-growing reflective plants, and f-whitening roofs and other building. Source:(Caldeira et al., 2013)

1.3. The IPCC's assessment

According to the IPCC Fifth Assessment Report (Kaito et al., 2000), SRM techniques "are associated with many uncertainties, side effects, risks and shortcomings" and "raise questions about the costs, risks, governance, and ethical implications of development and deployment."

In addition, IPCC AR5 states that "SRM will not prevent non-warming CO_2 impacts on ecosystems and ocean acidification." This assessment is supported by the recent IPCC Special Report on Global Warming of 1.5°C. They noted that SRM action is "subject to significant uncertainties and knowledge gaps, as well as significant risks, institutional and social constraints in terms of governance, ethics and impacts on sustainable development".

1.4. Different types of GeoMIP6

The Geoengineering Model Intercomparison Project Phase 6 (GeoMIP6) is a new set of climate model experiments for the Geoengineering Model Intercomparison Project (GeoMIP). These experiments build on previous GeoMIP simulations and aim to address several other important topics, including key uncertainties in extreme events, the use of geoengineering as part of a range of responses to climate change, and the relatively new idea of thinning cirrus clouds to allow more

of the longwave radiation to escape to space. The newly proposed experiments are G1ext, G6sulfur, G6solar and G7cirrus (Kravitz et al., 2015).

1.4.1. G1ext

This experiment consists of instantaneously quadrupling of CO_2 concentration, relative to pre-industrial levels and a reduction of the solar constant to counteract this extended 50 year forcing. **Figure 4** shows the schematic representation of the G1ext experiment. In G1ext, the average global radiative forcing due to CO_2 is offset by a reduction in the solar constant for 100 years.

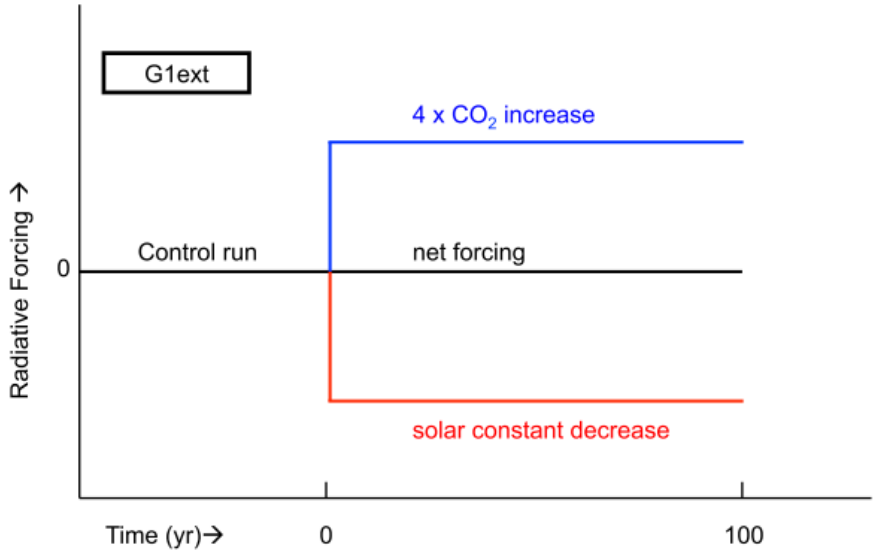

Figure 4: Schematic of experiment G1ext. Source: (Kravitz et al., 2015)

1.4.2. G6sulfur

In the G6sulfur experiment (**Figure 5**), sulphate aerosol precursors are injected into the equatorial stratosphere to reduce the radiative forcing of the high forcing ScenarioMIP (SSP5-8.5) to that of the medium forcing ScenarioMIP (SSP2-4.5). Geoengineering is simulated over the years 2020 to 2100. The simulations are performed as if the aerosols or aerosol precursors were emitted along a line from 10°S to 10°N along a single degree of longitude (0°). The introduced aerosols or aerosol precursors are uniformly distributed in the model layers between 18 and 20 km.

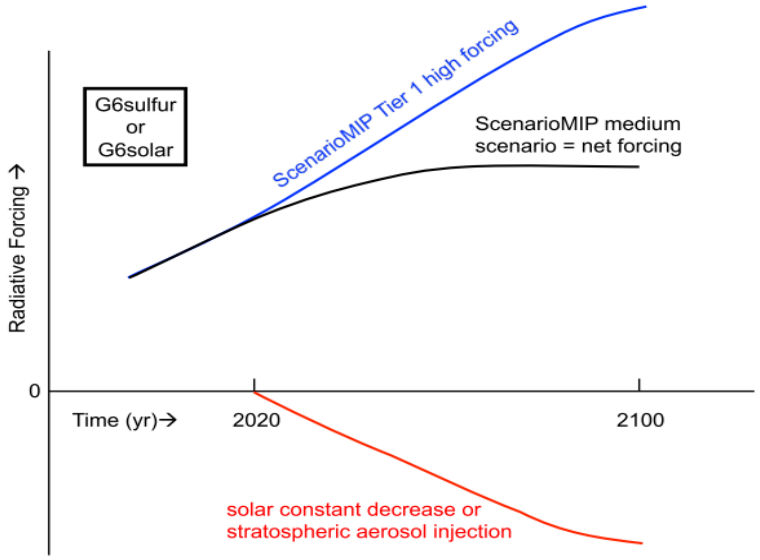

Figure 5 : Schematic of experiments G6sulfur and G6solar. Source: (Kravitz et al., 2015)

1.4.3. G6solar

G6solar is like a parallel experiment to G6sulfur. It uses the same configuration as G6sulfur, but geoengineering is done by reducing solar irradiance by altering solar constant in the model (**Figure 5**). The differences between the models in the spatial distribution of forcing are likely to be smaller than in G6sulfur, providing useful information on the effects of uncertainties in stratospheric sulphate aerosol transport.

1.4.4. G7cirrus

The simulation in G7cirrus consists of increasing the cirrus seeding rate by adding a local variable that replaces (at all locations where the temperature is below 235K) the ice mass mixing ratio in the calculation of the seeding rate with a value that is eight times the original ice mass mixing ratio. Cirrus seeding simulations begin in 2020 and continue until 2100 (**Figure 6**).

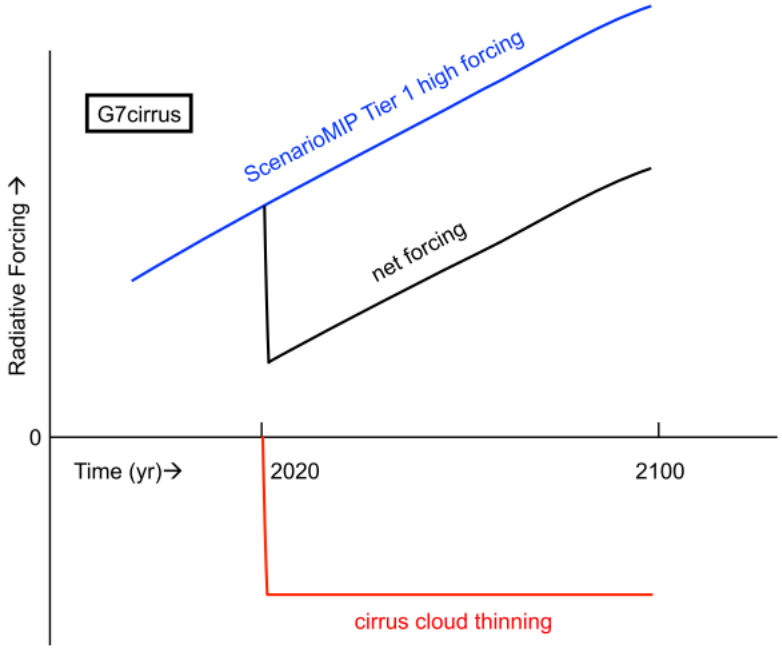

Figure 6 : Schematic of experiment G7cirrus. Source: (Kravitz et al., 2015)

1.5. Geoengineering research

In recent years, a number of scholars have engaged in the research into the physical mechanisms of geoengineering and its effects. For example, Kuswanto et al. (2021) investigates the potential impacts of stratospheric sulphate aerosol injection (SAI) on the change in mean and extreme temperatures over the Indonesian Maritime Continent. They show that SAI could reduce some of the negative impacts of climate change caused by temperature.

Geoengineering using sulfate aerosols is predicted to accelerate the hydroxyl-catalysed cycle of ozone destruction and lead to significant ozone depletion, although halogen concentrations will be much lower in the future (Heckendorn et al., 2009). Therefore, changes in stratospheric and tropospheric ozone need to be considered when designing SRM experiments, as it plays an important role in regulating UV exposure and air quality (Nowack et al., 2016).

Ecosystems play a number of important roles for the Earth. Indeed, the world's terrestrial and aquatic ecosystems are critical to human well-being and economic prosperity. They produce food and energy, regulate water supply and climate, provide resistance to disease and recycle waste (Lhomme et al., 2020). However, with the new proposal to combat climate change, some researchers like Russell et al. (2012) and Zarnetske et al. (2021) have investigate on the impact of

geoengineering on the ecosystem. They showed that geoengineering could have negative impact our ecosystem.

In Africa, researchers focused on changes in mean and extreme temperature, in water availability and in extreme precipitation, i.e., climate variables that determine the key climate risks. For instance, Pinto et al. (2020) investigated on the potential impact of SRM (Solar Radiation Management) on the mean and extreme temperatures and precipitation over Sub-Saharan Africa and found that SRM could significantly reduce the mean and extreme temperature. Also, Da-Allada et al. (2020) found that Stratospheric aerosol geoengineering could have a negative impact on the West African Summer Monsoon precipitation, which would be due to the decrease in the thermal contrast between land and sea at the lower level. This would lead to a weakening of the monsoon circulation and a northward shift of monsoon precipitation. In the same perspective, precipitation in the Middle East, North Africa and the Mediterranean will most likely decrease sharply (Karami et al., 2020). On the other hand, (Abiodun et al., 2021) showed that solar geoengineering activities could reduce the risk of a severe drought. They found that SAI intervention could offset climate change impacts on temperature that would overcompensate for impacts on precipitation and thus impose a climate water balance deficit.

The climate impact of SRM is often modeled by simply reducing the solar constant. Several studies have assessed the climate response to SRM by uniformly reducing the solar constant and stratospheric aerosols. For instance (Kalidindi et al., 2015) found that while the global mean diffuse radiation increased, the direct radiation during sulfate aerosol SRM decreased.

Geoengineering is considered as a new proposal to complement more conventional methods of climate mitigation, including renewable energy (The Royal Society, 2009). Some studies have shown that geoengineering would affect the potential of all direct and indirect solar renewable energy, including biomass, hydro, wind, as well as photovoltaic and solar thermal energy conversion (Moriarty & Honnery, 2013). West Africa has significant hydropower potential and renewable energy is an entry point to the green economy. Fewer quantitative studies have been published on the impacts of solar geoengineering on renewable energy. It is therefore important to investigate what impacts solar geoengineering could have on renewable energy.

Chapter 2: STUDY AREA, DATA AND METHOD

This section presents data and the method used in this study. The study area has been chosen because of its vulnerability to climate change and to better see the impact of solar geoengineering.

2.1. Study area

The study focuses on the region of West Africa. It is defined in this study as the region located between latitude 0-20° N and 20° W-20° E and divided into three climatic zones: Guinea (4-8° N), Savannah (8-12° N), and the Sahel (12-16° N) according to (Abiodun et al., 2012) (**Figure 7**).

The West African region has a vast renewable energy potential to meet unmet electricity demand and achieve universal access to electricity while supporting the region's transition to low carbon growth. According to IRENA's (International Renewable Energy Agency) analysis, 230 gigawatts (GW) of solar PV and wind alone is possible in the region, which could represent a combined share of 50 per cent of total capacity by 2040.

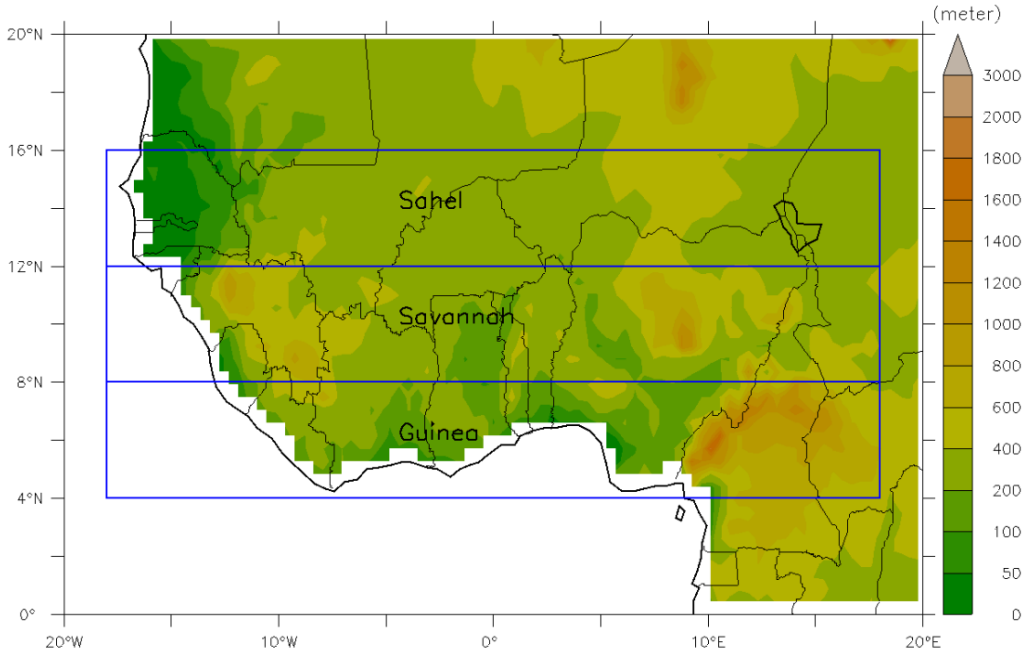

Figure 7: study domain, showing West Africa topography with its three climatic zones: Gulf of Guinea (Guinea), Savannah, and Sahel.

2.2. Data

This study used three different datasets. The first is the Geoengineering Model Intercomparison Project Phase 6 (GeoMIP6), specially the G6sulfur experiment. The second is from the Coupled Model Intercomparison Project Phase 6 (CMIP6; Eyring et al., 2016). CMIP6 is a new generation model of CMIP phases that provides large-scale coordinated simulations from state-of-the-art Global Climate Models (GCMs). From both datasets, we retrieved monthly surface-downwelling shortwave radiation (rsds), air temperature (tas) and wind speed (wspd; at 10m above the ground level). For each dataset, the historical and projected experiments were used. Three different scenarios of climate change are considered in this study:

1. The Shared Socio-Economic Pathway 2-4.5 (SSP2-4.5)

SSP2-4.5 represents an intermediate scenario in which the current climate change trend stays unchanged, resulting in a forcing path of 4.5 Wm^{-2} associated with socio-economic reasons at the end of the century. CO_2 emissions hover around current levels before starting to fall mid-century, but do not reach net-zero by 2100. Socio-economic factors follow their historic trends, with no notable shifts. Progress toward sustainability is slow, with development and income growing unevenly. In this scenario, temperatures rise 2.7°C by the end of the century (IPCC, 2021).

2. The Shared Socio-Economic Pathway 5-8.5 (SSP5-8.5)

SSP5-8.5 represents the scenario where no GHG emission policy is applied, resulting in intensive fossil fuel consumption, resulting in a forcing path of 8.5 Wm^{-2} associated with socio-economic reasons in 2100. This is a future to avoid at all costs. Current CO_2 emissions levels roughly double by 2050. The global economy grows quickly, but this growth is fueled by exploiting fossil fuels and energy-intensive lifestyles. By 2100, the average global temperature is a scorching 4.4°C higher (IPCC, 2021).

3. G6sulfur

The G6sulfur experiment injects stratospheric sulphate aerosol pollutants into the model to reduce the net anthropogenic radiative forcing from the high forcing scenario to the medium forcing scenario (Kravitz et al., 2015).

Due to variable that we used , only 3 CMIP6 and GeoMIP6 models were available at the time of this study. **Table 1** displays more details on the two datasets used in this study with information on their institution (modelling centres), model name and horizontal grid resolution of each model. Finally, the third dataset is the ERA5, used for the model evaluation. ERA5 is the fifth generation of the European Centre for Medium-Range Weather Forecasts (ECMWF) global climate reanalysis (Hersbach et al., 2019). ERA5 has a horizontal grid spacing of about 31 km and the time period spans from 1979 to the present. It was built from the Era-Interim dataset and provides a high spatial and temporal resolution reference data. Note that, although ERA5 is an advanced dataset with assimilation of observations, improving on several aspects of the previous ERA-Interim product, it is still a model product characterized by some systematic biases (Dullaart et al., 2020). Monthly rsds, tas, and wspd were obtained from the ECMWF platform for the period 1985-2014.

Table 1: Global circulation models (GCMs) used with the institution name and their native grid number in this study

Institution	**Global circulation model (GCM)**	**Longitude**	**Latitude**	**References**
Max Planck Institute for Meteorology (MPI-M)	MPI-ESM1-2- HR	384	192	Jungclaus et al. (2019), Niemeier et al. (2019a)
	MPI-ESM1-2- LR	192	96	Schupfner et al. (2021), Niemeier et al. (2019b)
Met Office Hadley Centre (MOHC)	UKESM1-0-LL	192	144	Tang et al. (2019), Jones et al. (2019)

2.3. Model Description

Three models were used to assess the potential impact of geoengineering on renewable energy, as shown in **Table 1**. Not all participating models have stratospheric aerosols through direct SO_2 injection. Only the UKESM1-0-LL model has an interactive microphysical aerosol model in the stratosphere (Tilmes et al., 2021), (Sellar et al., 2019). The model injects SO_2 uniformly at a single longitude (0°) between 10°N and 10°S and at altitudes of 18 and 20 km (Visioni et al., 2021), while MPI-ESM determines its aerosol distribution from the simulation described in (Niemeier &

Schmidt, 2017), (Niemeier et al., 2020).

2.4. Method

The different drivers of solar and wind energy such as rsds, tas and wspd from CMIP6 simulations and its ensemble mean (referred to as Rmean) are evaluated against ERA5 observational data in the reference climate period (1985-2014). The Rmean is computed from the mean of the three models. The Photovoltaic power potential (PVP) and wind power density (WPD) are evaluated for reference period as well. All the assessments were made at the annual mean scale, and we also evaluated the performance of the CMIP6 models in reproducing the annual cycle of rsds, tas, wspd, PVP and the WPD. We also calculated the deviation between simulation and ERA5 of each variable. We also used the Taylor diagram to compare the simulations and observations. The Taylor diagram is a useful tool for evaluating model performance (Simão et al., 2020). The Taylor diagram provides a precise statistical summary of the agreement between the models and observations in terms of correlation, root-mean-square difference and normalized standard deviation.

We analysed the future projected changes in the solar and wind energy and their different drivers under three scenarios, SSP5-8.5, SSP2-4.5, and G6 sulfur. We used two time periods: 2021-2050 and 2070-2099, representing the near future and the far future respectively. These scenarios are compared to the historical reference period (1985-2014). The projected changes are the difference between the future period and the reference period. The projected changes in rsds, tas, wspd, and WPD are expressed in absolute change while the PVP are in relative change. In addition, the significant changes in the projection are assessed by computing the 90% confidence level of the t-test of the individual model and variable.

2.4.1. Photovoltaic power potential (PVP)

The Photovoltaic power potential is the average electricity production (in kWh) expected over the lifetime of the system per kilowatt of installed photovoltaic capacity under standard test conditions (STC) for grid-connected PV systems without batteries. The energy model generated by the PV system is based on the power rating of the system, the temperature coefficient of the modules, the insolation, the air temperature and the wind speed. Likewise to previous study (Sawadogo et al., 2021), and following (Mavromatakis et al., 2010) the PVP can be expressed as follows:

$$\mathrm{PVP(t)} = \mathrm{Pr(t)}.\frac{\mathrm{rsds(t)}}{\mathrm{rsds_{STC}}} \quad (1)$$

where rsds is the surface-downwelling shortwave radiation at the location site, $\mathrm{rsds_{STC}}$ is the solar irradiance of 1000W/m^2 at standard test conditions (STC). Pr(t) is the power ratio; it accounts for changes in photovoltaic cell efficiency due to temperature changes (Jerez et al., 2015) and is defined as:

$$\mathrm{Pr(t)} = 1 + \gamma.[\mathrm{T_{cell}} - \mathrm{T_{STC}}] \quad (2)$$

where T_{cell} is the temperature of the PV and T_{STC} is the ambient air temperature at STC i.e., 25 °C. γ is a constant and depends on the type of PV cells. For the silicon module, the value is taken assumed to be -0.005 °C^{-1} (Jerez et al., 2015). T_{cell} is modelled as a function of solar irradiance, air temperature, wind speed and relative humidity. According to (Sawadogo et al., 2021), the contribution of wind speed and relative humidity to changes in PVP in Africa is negligible. Hence, T_{cell} is formulated as a function of solar irradiance (rsds) and air temperature (tas) as follows:

$$\mathrm{T_{cell}(t)} = C_1 + C_2.\mathrm{tas(t)} + C_3.\mathrm{rsds(t)} \quad (3)$$

With C_1 = 3.75 °C, C_2 = 1.14, and C_3 = 0.0175 °C m^2 W^{-1} (Sawadogo et al., 2021).

2.4.2. Wind power density (WPD)

Wind power density (WPD) is a quantitative measure of the wind energy available at any given location. It is the average power available per square meter of swept area of a turbine (W/m^2), and is expressed in the following equation:

$$\mathrm{WPD} = \frac{1}{2}\,\rho\,\mathrm{V^3} \quad (4)$$

where V is the wind speed at the adjusted-to-turbine hub height (here as 100 m), and ρ is the air density (standard conditions are assumed for ρ with a constant value of 1.225 kg m^{-3}). To calculate the WPD, most studies extrapolate the surface wind speed of 10 meters to the desired hub height of the turbine. There are many ways to extrapolate the 10 m surface wind measurement to the

turbine hub height. The power law method (Akinsanola et al., 2021b) defined in equation (5), used in this study assumes that wind speed at a certain height z is approximated as follows:

$$\mathrm{wspd}(z) = \mathrm{wspd}(z_{ref}) \left(\frac{z}{z_{ref}}\right)^{\alpha} \quad (5)$$

where z is the height at turbine hub height (taking as 100 m), z_{ref} is the reference height, wspd(z_{ref}) is the wind speed at z_{ref}, and α is the power law exponent. The near-surface wind speed at 10 m is used as the reference height wind speeds in this study and we assume that α = 1⁄7. This method to compute WPD has been used in previous studies (Akinsanola et al., 2021 and Sawadogo et al., 2021).

Chapter 3: RESULTS AND DISCUSSIONS

This chapter presents and discusses our findings. we have divided our results into two parts. first, we evaluate the models used, and then we analyse the projected changes by variable and by energy potential in a climate with and solar geoengineering.

3.1. Model evaluation

The spatial distribution of the annual average of rsds, tas, and wspd is shown in **Figure 8** for ERA5 (observation), CMIP6 models (MPI-HR, MPI-LR, UKESM), and their ensemble mean (Rmean) for the reference period (1985-2014). For each variable, all three models and the Rmean reproduce well the spatial distribution observed by the ERA5, with the spatial correlation ranging from 0.81 to 0.97. In agreement with the observation, the highest values of rsds (300 W/m^2) are observed in the Sahel zone with a high annual mean tas of about 30°C. The highest rsds values in the Sahel could be due to the low cloud cover throughout the year. The minimum rsds is observed in the Guinea zone with an average value of 160 W/m^2. The Guinea zone is known as a cloudy area where most thunderstorms occur. There is a consistency between rsds and tas in the region. When rsds is high (low), the tas is high (low). The wind speed is dominating the Sahelian zone with a maximum magnitude of about 7.2 m/s, decreasing in the coastal areas. This low wind magnitude observed over the Gulf of Guinea is due to higher vegetation cover, with the effect of roughness on the aerodynamic performance reducing the wind speed (Guerri, 2012).

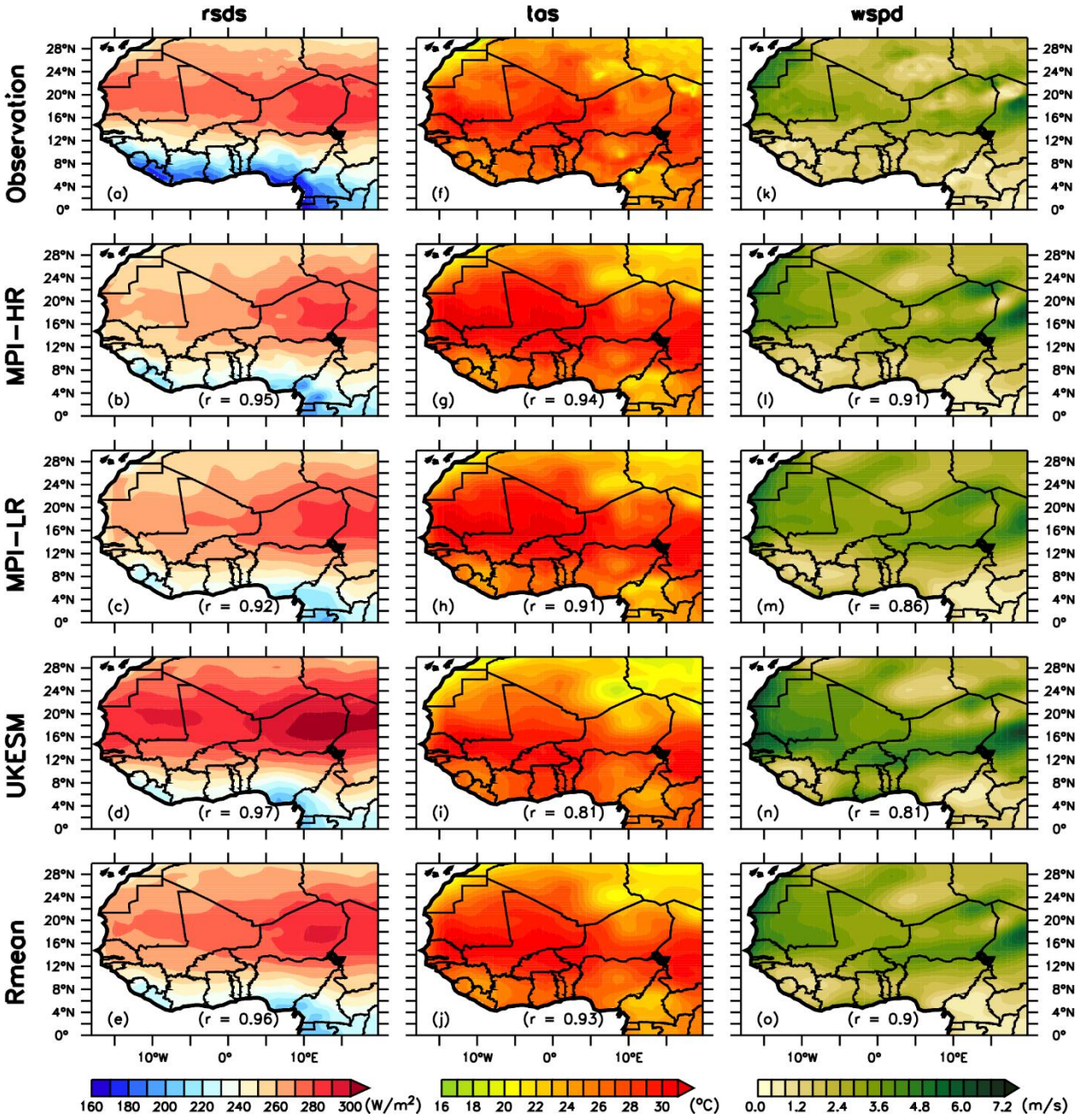

Figure 8: Spatial distribution of the annual mean of solar irradiance (rsds), temperature (tas), and wind speed (wspd) for the reference period (1985-2014) from three CMIP6 models (MPI-HR, MPI-LR, UKESM) and their ensemble mean (Rmean). The spatial correlation between observation and simulation is shown in parentheses.

The discrepancies between simulations and observations of annual mean rsds, tas, and wspd for different models are shown in **Figure 9**. Although the models correlate well with the observed data, some considerable biases are evident in the simulations. All simulations show negative (positive) bias indicating underestimation (overestimation) of the different variables. For example, MPI-HR, MPI-LR and Rmean overestimate (i.e., positive bias) rsds (up to 40 W/m2 along the Guinea coast) and underestimate (i.e., negative bias) it over the Sahel (up to 10 W/m2). This is in contrast to UKESM simulation, which overestimates rsds over most of West Africa. Most simulations underestimate the tas in the Guinea zone (in the order of -1 to 1°C) and overestimate it in the Sahel zone (up to 2°C). Contrary to the UKESM model which shows the opposite tendency. The simulated wspd shows a warm bias over the West African region of about 1.5 m/s. These simulated biases may be due to poor representation of optical clouds properties or/and aerosols in the climate models. Several studies have shown that the representation of cloud properties is a significant challenge in climate models. They suggest that biases are due to inadequacies in the physical parameters associated to cloud properties rather than the model's treatment of resolution, ocean, and chemistry (Chen et al., 2022).

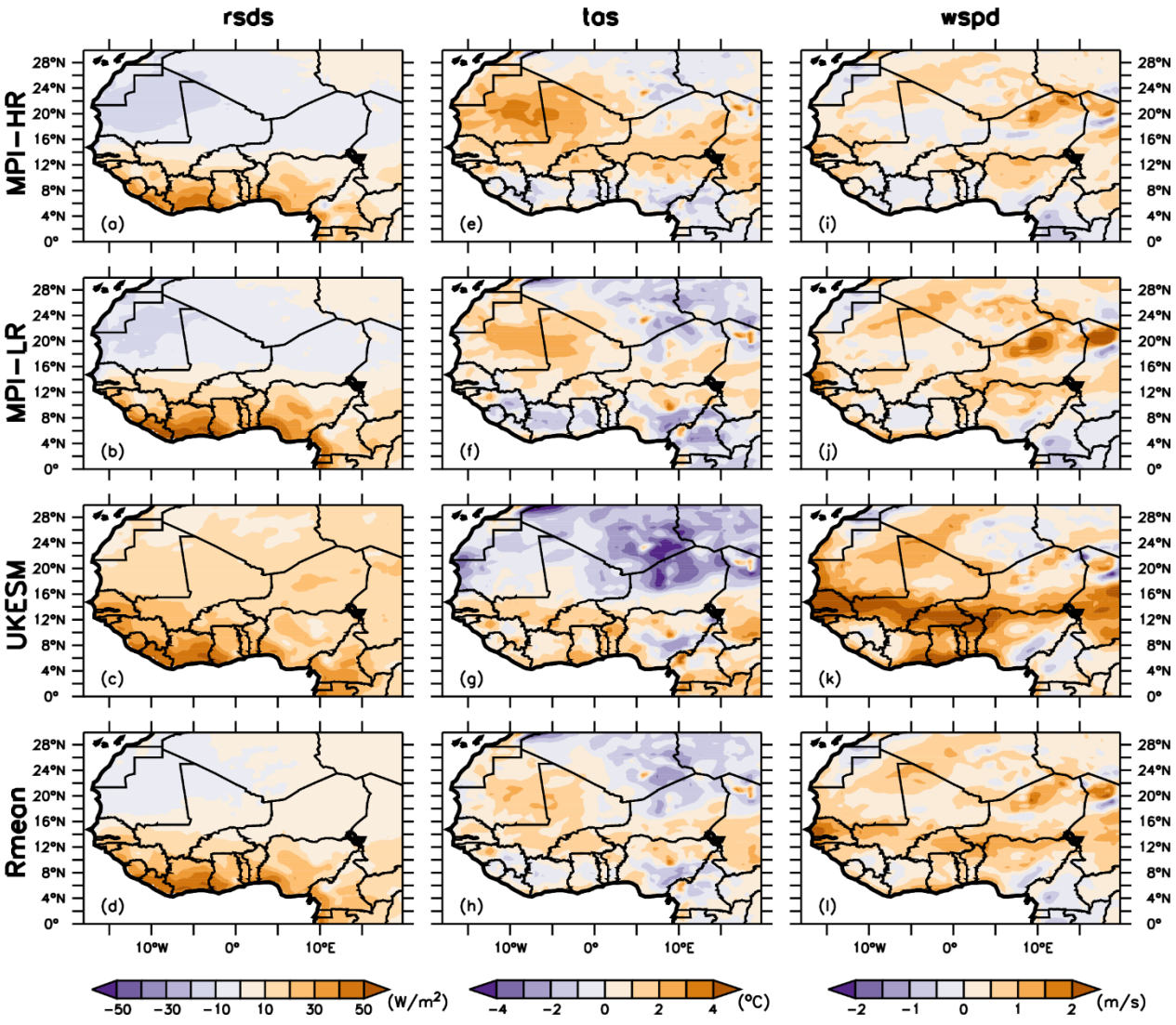

Figure 9: Bias (simulation minus observation) of the annual mean of solar irradiance (rsds), temperature (tas), and wind speed (wspd) for the reference period (1985-2014) of three CMIP6 models (MPI-HR, MPI-LR, UKESM) and their ensemble mean (Rmean).

Figure 10 shows that the models reproduce the observed annual cycle of the variables (rsds, tas, and wspd) in each climate zone. The simulations capture the maxima and minima of rsds, tas, and wspd over each zone with different magnitudes. In the Sahel zone, in agreement with the observations, the models simulate a maximum of rsds and tas during the hot season (Mar-April) and a minimum of rsds and tas during the peak of the rainy season (August). These maxima and minima are similar in the savannah and Guinea zones. The difference lies in the magnitudes, which are higher in the Sahel zone and drop to minimum values in the Guinea zone. The maximum peaks (minimum) of wind speed (wspd) are seen during the minimum peaks (maximum) of rsds and tas in the different regions. These results show a correlation between rsds, tas and wspd that is consistent with previous studies (Mann et al., 2004; Dos Anjos et al., 2015).

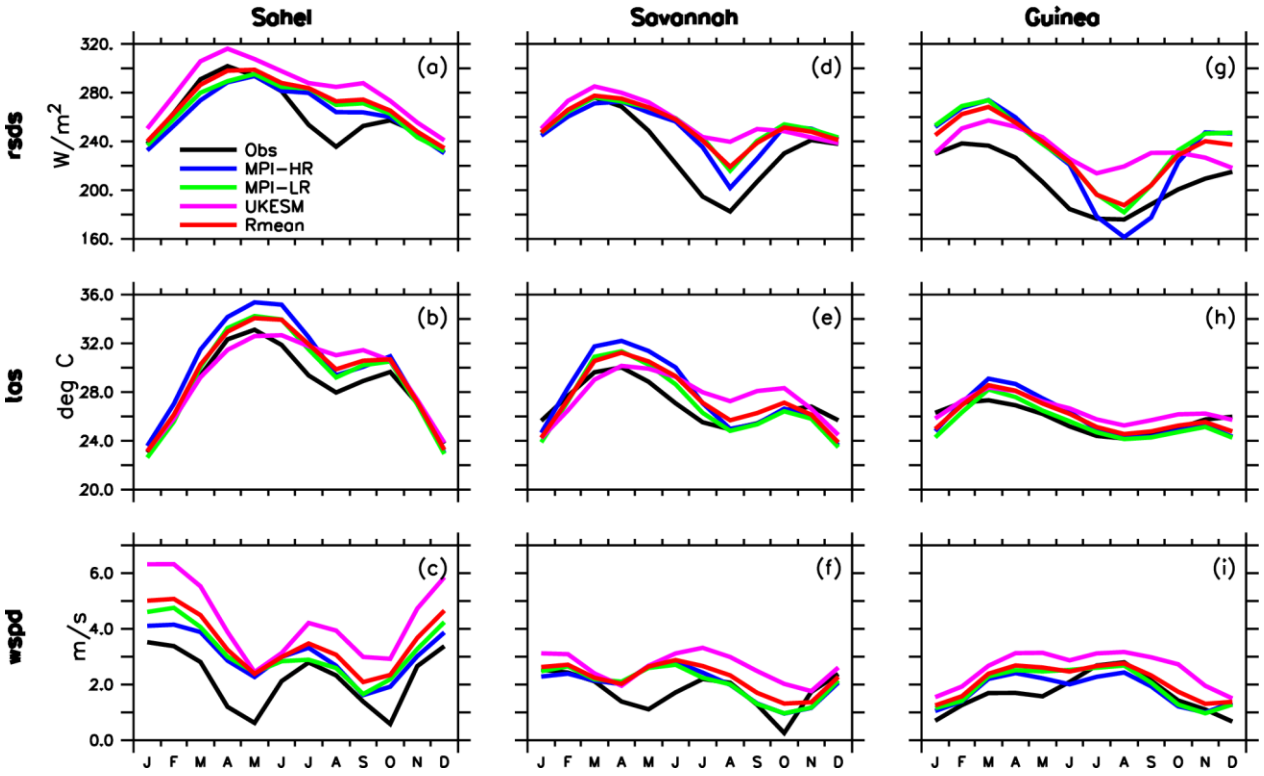

Figure 10 : Annual cycle of solar irradiance (rsds), temperature (tas), and wind speed (wspd) over the three West African zones (Guinea, Savannah, and Sahel) for the reference period (1985-2014) of the observation (Obs), three CMIP6 models (MPI-HR, MPI-LR, UKESM) and their ensemble mean (Rmean).

The models' simulations reproduce the spatial distribution of PVP and WPD over West Africa, with correlations of 0.91 to 0.97 and 0.71 to 0.84 respectively (**Figure 11**). The models follow the spatial distribution of rsds. Similarly, WPD also shows a maximum over the Sahel (about 180 W/m^2) and a minimum over Guinea zone, with the Rmean showing a positive bias of about 60 W/m^2 over the Sahel (**Figure 12e-h**). The simulated biases for the PVP are like those of the rsds (**Figure 12a-d**). The observed annual cycle of PVP over the Sahel, Savannah and Guinea areas is similar to that of the rsds (**Figure 13a-b**). It shows the highest PVP value (35%) during the dry season (Dec-Jan-Feb-Mar-April) when skies are clear and the lowest values (18%) during the rainy season (June-July-August) when the presence of clouds minimises rsds. The magnitude of WPD gradually decreases from the Sahel to the Guinea zone (**Figure 13d-f**).

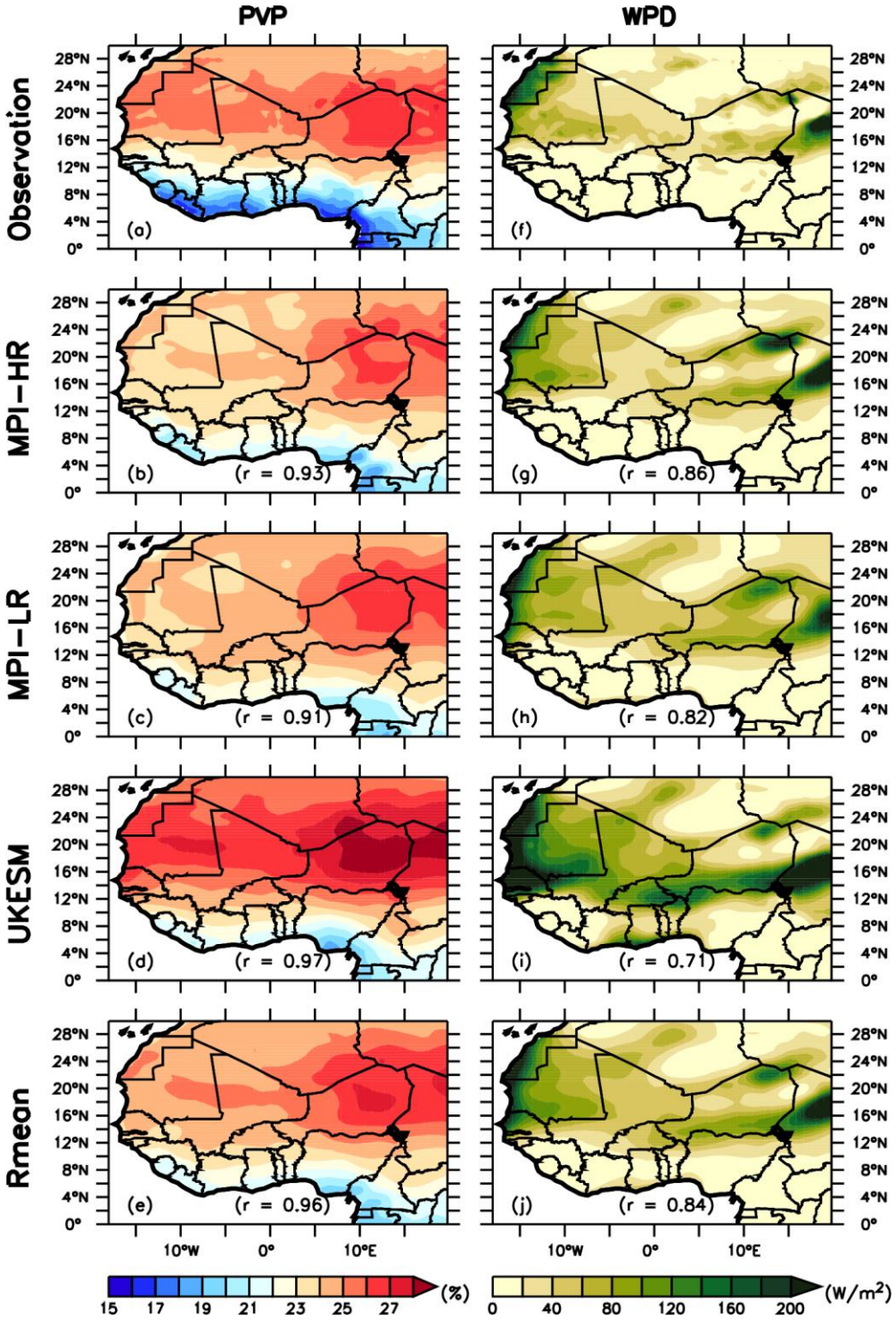

Figure 11 : Spatial distribution of the annual mean of PVP and WPD for the reference period (1985-2014) from three CMIP6 models (MPI-HR, MPI-LR, UKESM) and their ensemble mean (Rmean). The spatial correlation between observation and simulation is shown in parentheses.

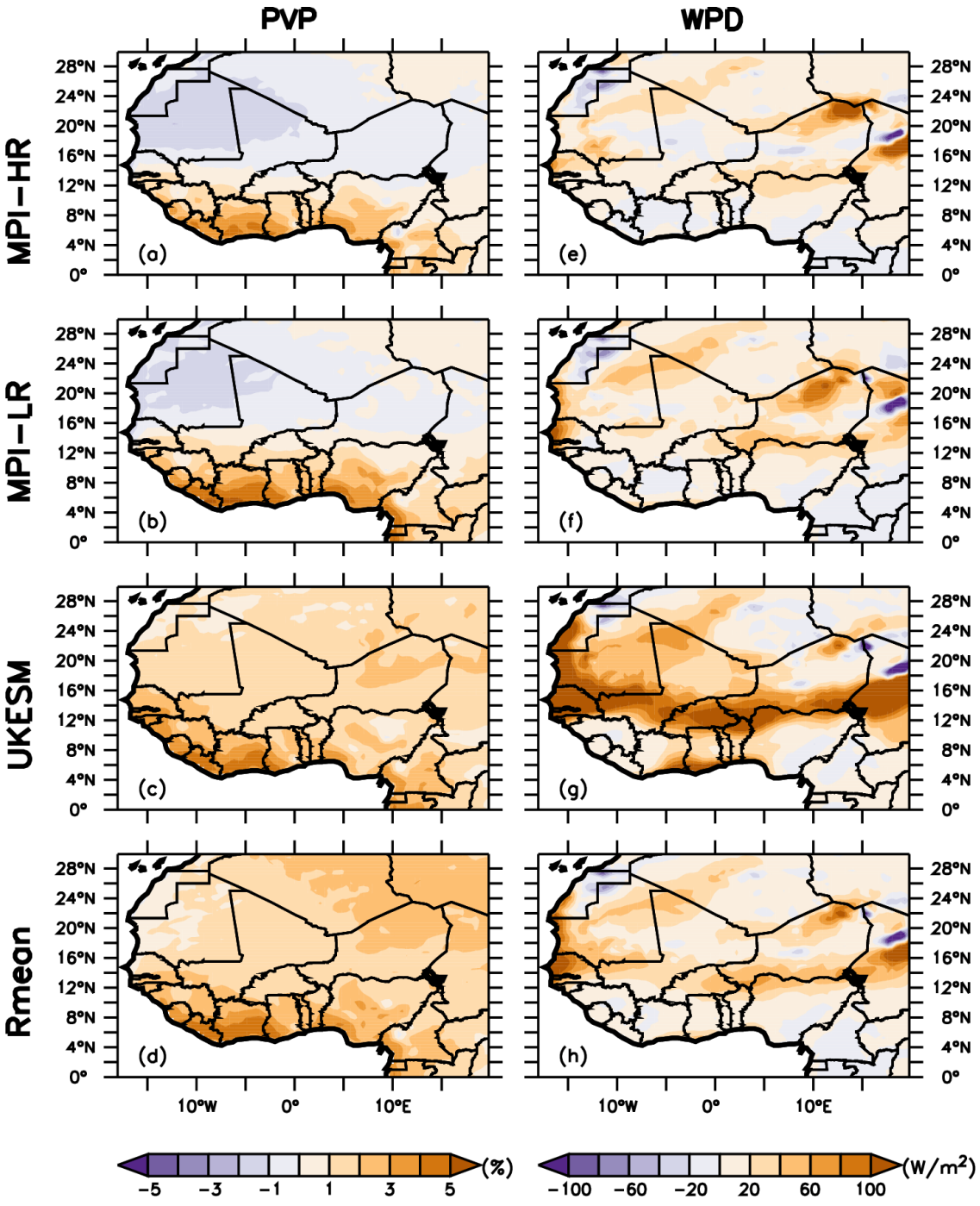

Figure 12: Bias (simulation minus observation) of the annual mean of PVP and WPD for the reference period (1985-2014) of three CMIP6 models (MPI-HR, MPI-LR, UKESM) and their ensemble mean (Rmean).

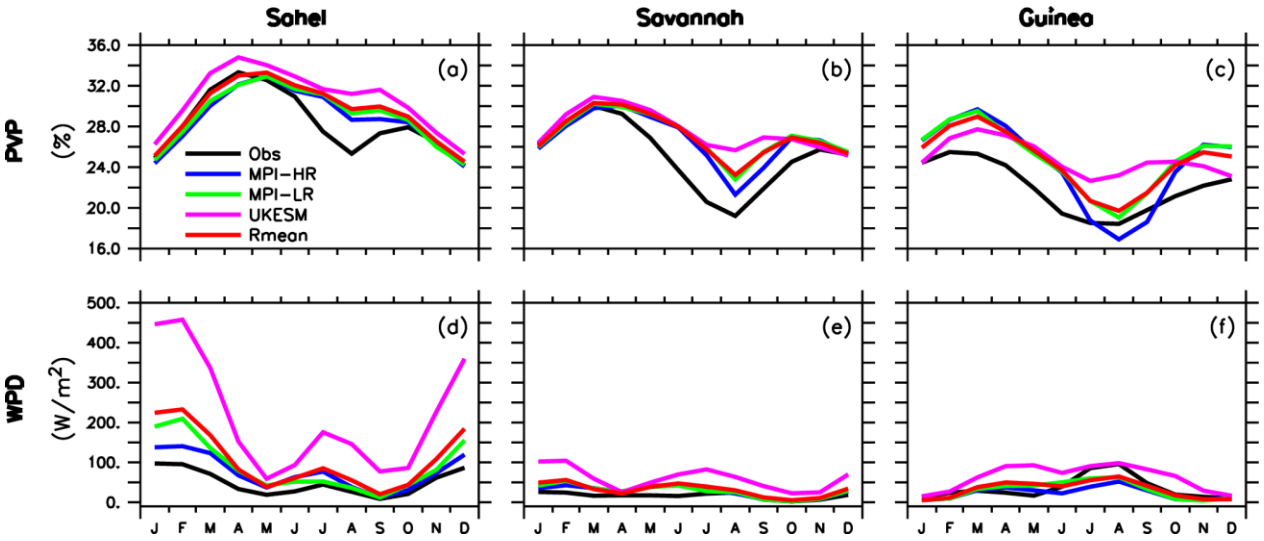

Figure 13: Annual cycle of PVP and WPD over the three West African zones (Guinea, Savannah, and Sahel) for the reference period (1985-2014) of the observation (Obs), three CMIP6 models (MPI-HR, MPI-LR, UKESM) and their ensemble mean (Rmean).

Figure 14 represents the Taylor diagram for rsds, tas and, wspd calculated over the three West African zones (Guinea, Savannah, and Sahel) of each model and its Rmean. For rsds, the simulations show high spatial correlations and a normalized standard deviation of less than 1 in Sahel and Savannah zones (**Figure 14a-b**). On the other hand, low correlations are observed in the Guinea zone (**Figure 14c**). The PVP also shows the same results (**Figure 15a-c**). As mentioned above, the representation of cloud properties in the climate models is a source of uncertainty in the simulations. As for temperature, the models show good correlations and standard deviations in all regions (**Figure 15d-f**). The same is true for wspd but with the difference that only the UKESM model shows a poor performance (**Figure 15g-i**). Similarity, the WPD shows the same results (**Figure 15d-f**).

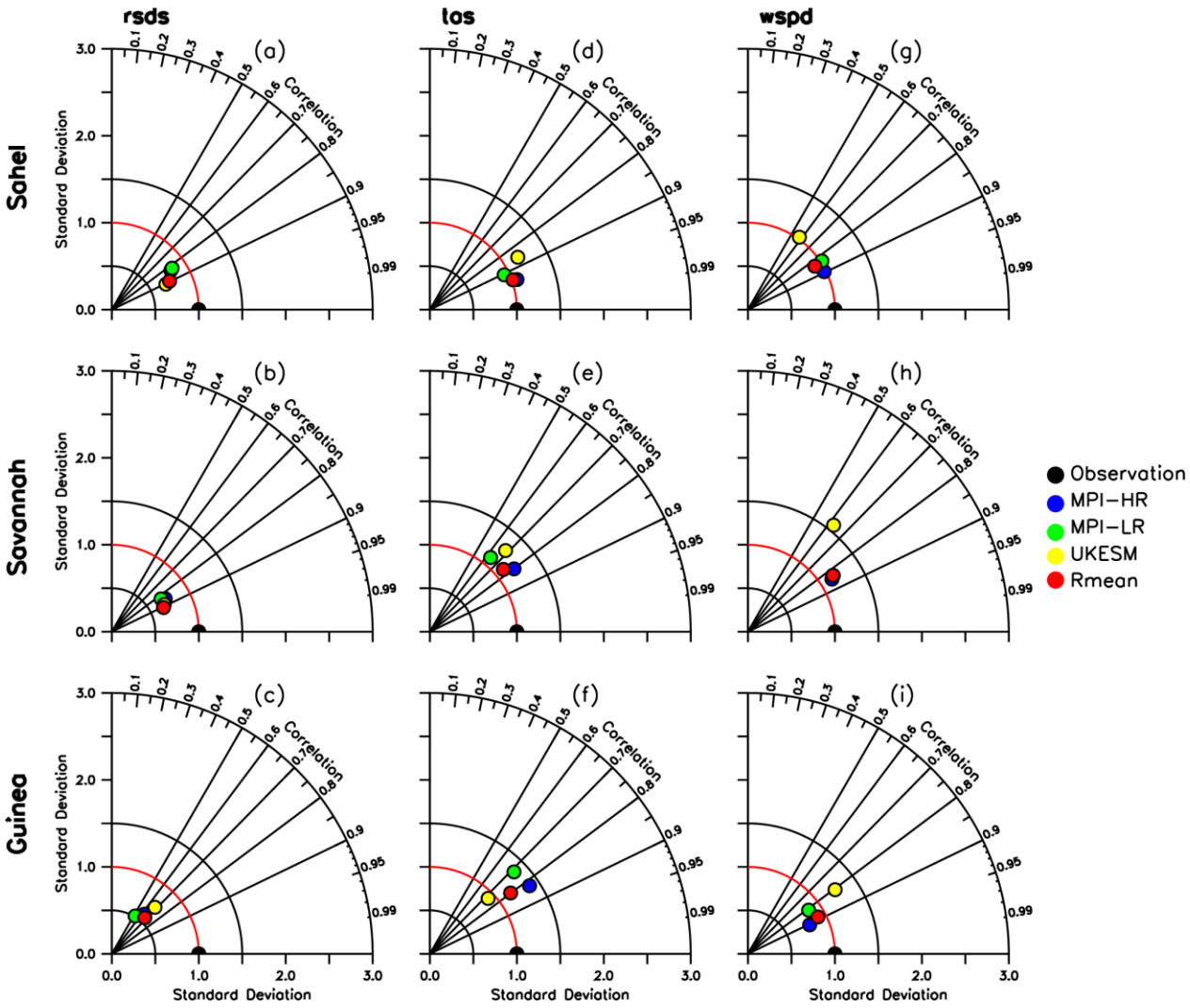

Figure 14 : Taylor diagrams of solar irradiance (rsds), temperature (tas), and wind speed (wspd) over the three West African zones (Guinea, Savannah, and Sahel) for the reference period (1985-2014) from three CMIP6 models (MPI-HR, MPI-LR, UKESM) and their ensemble mean (Rmean). The spatial correlation and normalised standard deviation are calculated for each simulation and for the Rmean.

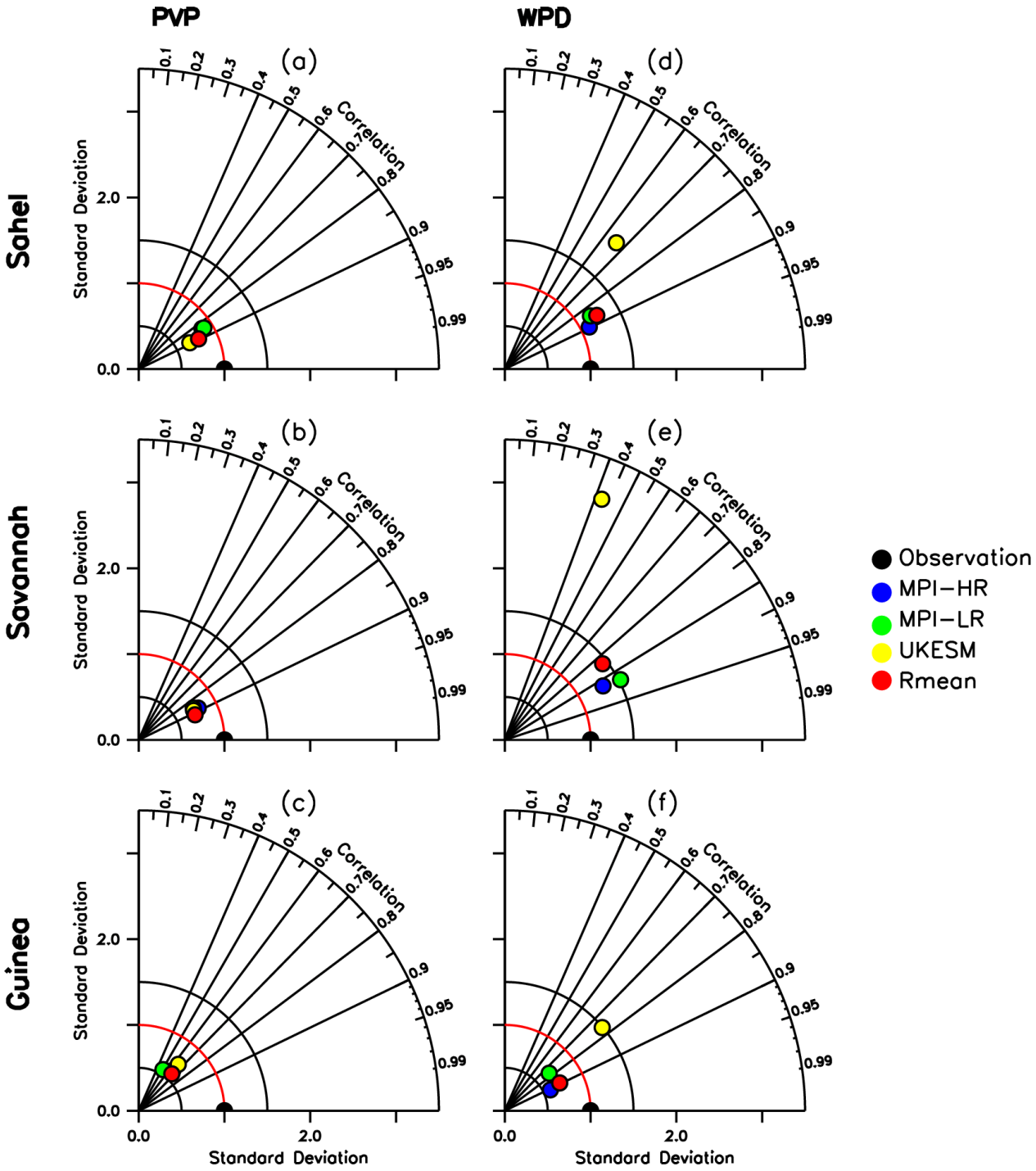

Figure 15 : Taylor diagrams of PVP and WPD over the three West African zones (Guinea, Savannah, and Sahel) for the reference period (1985-2014) from three CMIP6 models (MPI-HR, MPI-LR, UKESM) and their ensemble mean (Rmean). The spatial correlation and normalised standard deviation are calculated for each simulation and for the Rmean.

Briefly, we analyse the performance of the models used in this study. First, we highlight the spatial distribution and annual cycles of the different variables over West Africa. We then calculate the PVP and WPD and finally use Taylor diagrams to better evaluate our models. Despite all the observed biases, the simulations of the solar and wind variables capture well the atmospheric processes that influence the PVP and WPD over West Africa. We will now focus on the analyse of the projections, analyse them, and examine the impact of G6sulfur on solar and wind.

3.2. Climate projection

The aim of the G6sulfur experiment is to modify the simulations based on the high forcing scenario SSP5-8.5 to follow the evolution of the medium forcing scenario SSP2-4.5. The projections for the near future (2021-2050) do not show significant changes compared to the far future (2070-2099), where the changes are important. This can be explained by the fact that the G6sulfur experiments started at the beginning of the 21st century and it, therefore, takes a long time for changes to be projected. In the following, we will focus on far future projections.

3.2.1. Projected changes of the variables

Figure 16 shows the projected changes in annual mean temperature for the three models (MPI-HR, MPI-LR, UKESM) and their ensemble mean (Rmean) under the SSP2-4.5, SSP5-8.5, and G6sulphur scenarios in the far future. The changes are significant at the 90% confidence level over West Africa.

The SSP5-8.5 projections indicate an average temperature increase of about 4°C over West Africa, which is even higher in the Sahel zone. Only the UKESM model presents a temperature rise of 6°C over West Africa. These projections are driven by a high atmospheric CO_2 concentration in the order of 1135 ppm. So, in the future, with the anthropogenic activities we will assist a rapid temperature increase. The G6sulfur experiment shows a decrease in temperature compared to the SSP5-8.5 and SSP2-4.5 scenarios. Temperature drops to about -3°C across West Africa, hence the cooling effect (**Figure 16q-t**). The UKESM simulation shows a stronger cooling effect (about -4°C) compared to the other two simulations. This suggests that stratospheric aerosol injection could reduce the effect of global warming. For instance, during the natural phenomenon of the 1991 volcanic eruption of Mount Pinatubo in the Philippines, where sulphur particles were injected into the stratosphere, we observed an enhanced reflection of solar radiation by the particles into space,

which led to a decrease in the Earth's surface temperature of about 0.5 °C in the year following the eruption. This phenomenon has identified sulfur as a particle that could lower the Earth's global temperature. Previous studies have shown comparable results in Indonesia (Kuswanto et al., 2021).

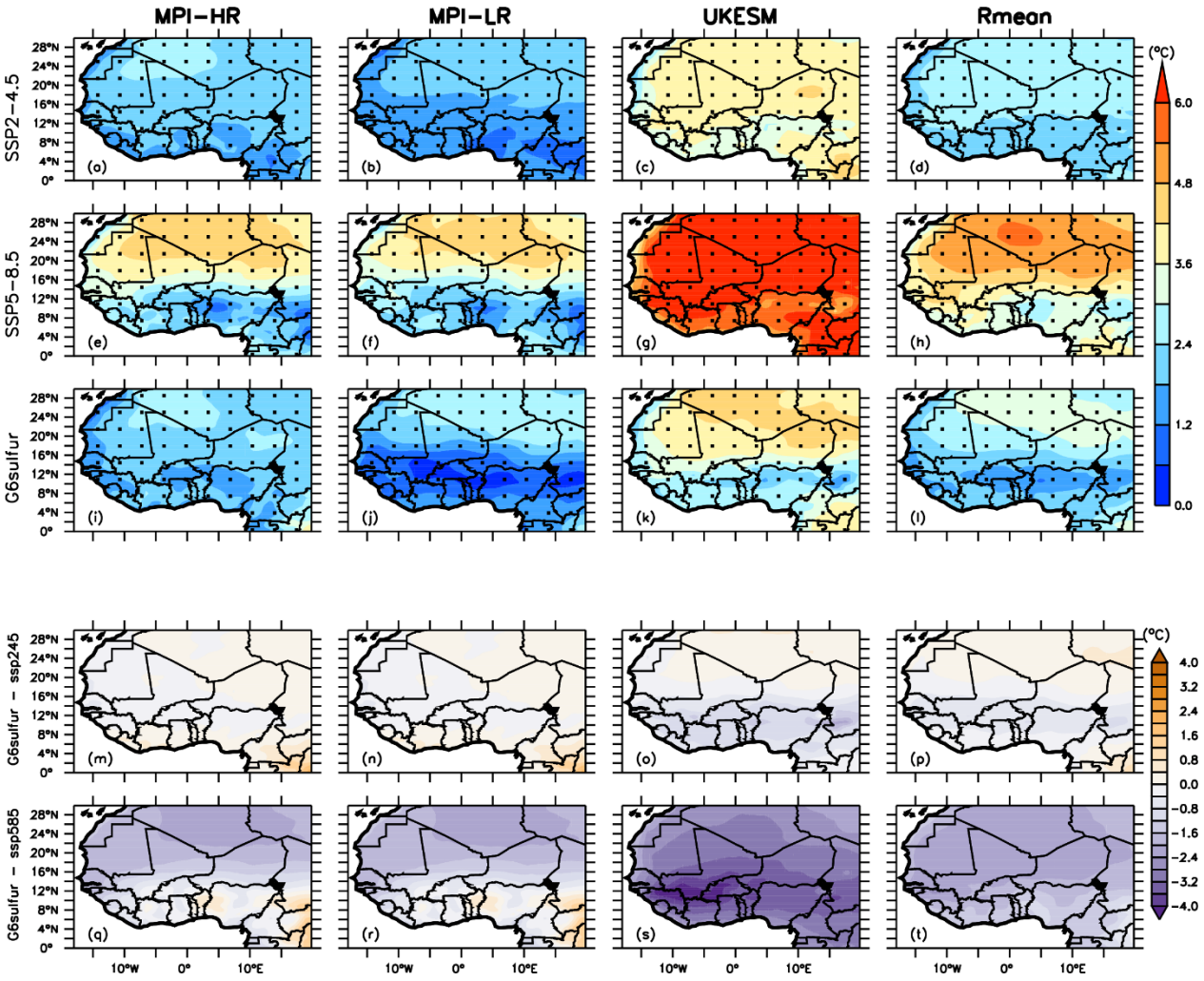

Figure 16 : Projected changes in annual mean temperature in the far future (2070-2099) of the three models (MPI-HR, MPI-LR, UKESM) and their ensemble mean (Rmean) under SSP2-4.5 (a-d), SSP5-8.5 (e-h) and G6sulfur (i-l) scenarios, the difference between G6sulfur and SSP2-4.5 (m-p), the difference between G6sulfur and SSP5-8.5 (q-t). The dotted lines indicate areas that are significant at the 90 % level using the Student t-test.

The projected changes in mean annual solar irradiance shown in **Figure 17**, indicate a decrease of about 20 W/m^2 in the Gulf of Guinea and 4 W/m^2 in the Sahel zone for the SSP5-8.5 projection. For G6sulfur the radiation increases compared to the SSP5-8.5 projection for MPI-HR and MPI-LR simulations. In the UKESM, a decrease of solar irradiance is observed, compared to the SSP5-8.5 scenario. The difference between the G6sulphur and the SSP5-8.5 projections is characterized by an increase in solar irradiance magnitude of 20 W/m^2 in the Savannah and Gulf of Guinea regions and a decrease in the Sahel region mainly in MPI-HR and MPI-LR simulations (Fig.14 q-t). The decrease in solar irradiance is only observed in the UKESM simulation. The discrepancy between the three simulations could be attributed to the interactive microphysical aerosol model in the stratosphere used in the UKESM simulation (Tilmes et al., 2021).

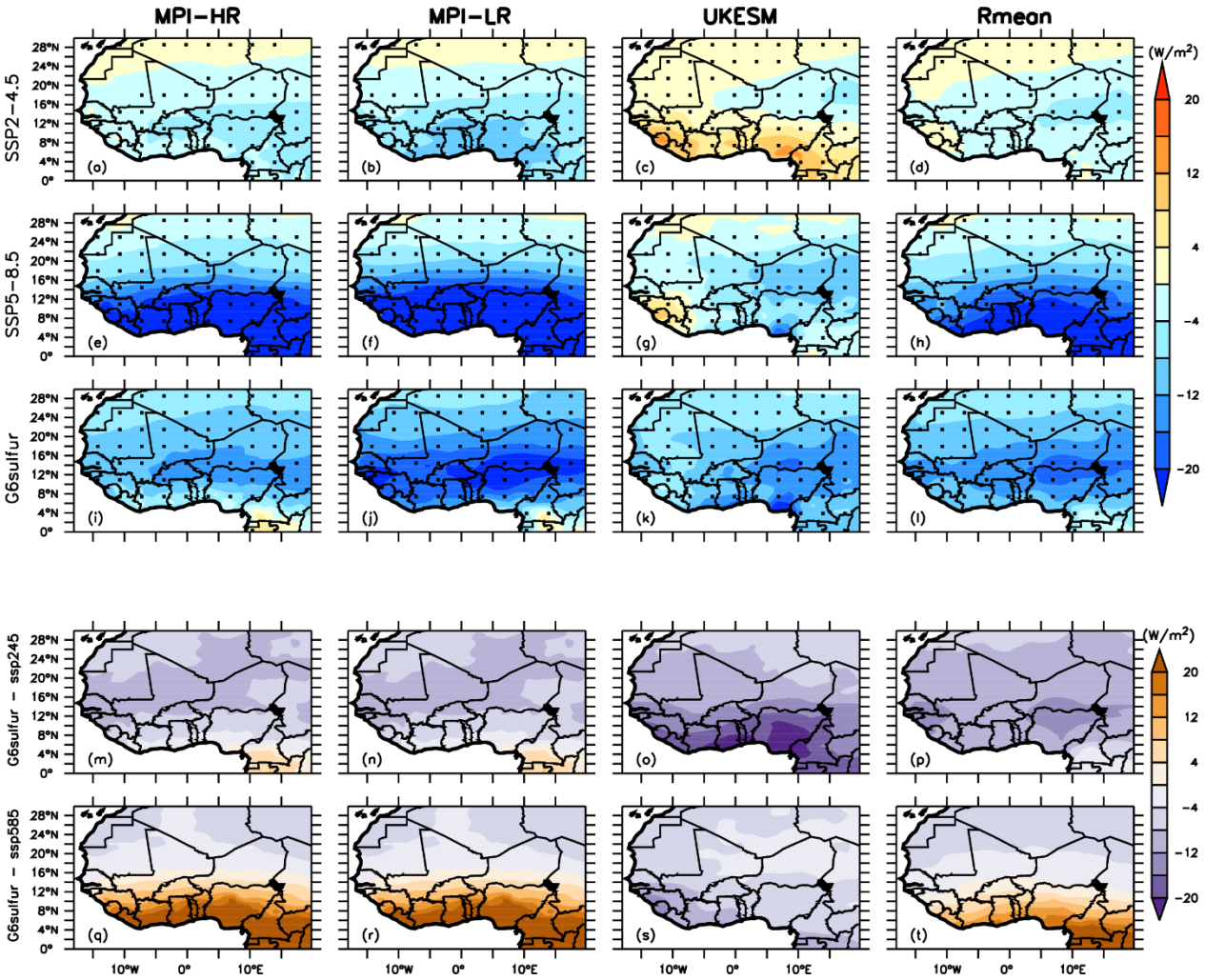

Figure 17 : Projected changes in annual mean solar irradiance in the far future (2070-2099) of the three models (MPI-HR, MPI-LR, UKESM) and their ensemble mean (Rmean) under SSP2-4.5 (a-

d), SSP5-8.5 (e-h) and G6sulfur (i-l) scenarios, the difference between G6sulfur and SSP2-4.5 (m-p), the difference between G6sulfur and SSP5-8.5 (q-t). The dotted lines indicate areas that are significant at the 90 % level using the Student t-test.

The projected changes in annual mean wind speed for the three models (MPI-HR, MPI-LR, UKESM) and their ensemble mean (Rmean) under the SSP2-4.5, SSP5-8.5, and G6sulphur scenarios in the far future is presented in **figure 18**. The SSP5-8.5 projection shows an average wind speed increase of 2 m/s in the Sahel zone and 1 m/s over the Guinea zone. The objective of the GeoMIP simulations is to reduce the amount of solar radiation reaching the land and sea surface by injecting SO_2 particles into the stratosphere. SO_2 particles could reflect some of the incident radiation back into the atmosphere. As a result, it will heat the Earth less, and thus reduce the land-sea thermal contrast at low altitudes. The reduction of the land-sea thermal contrast leads to weaker winds (Da-Allada et al., 2020). In agreement with (Alamou et al., 2022), they found that the general circulation could, therefore, play a key role in the weakening of the ocean basin winds under G6sulfur activity.

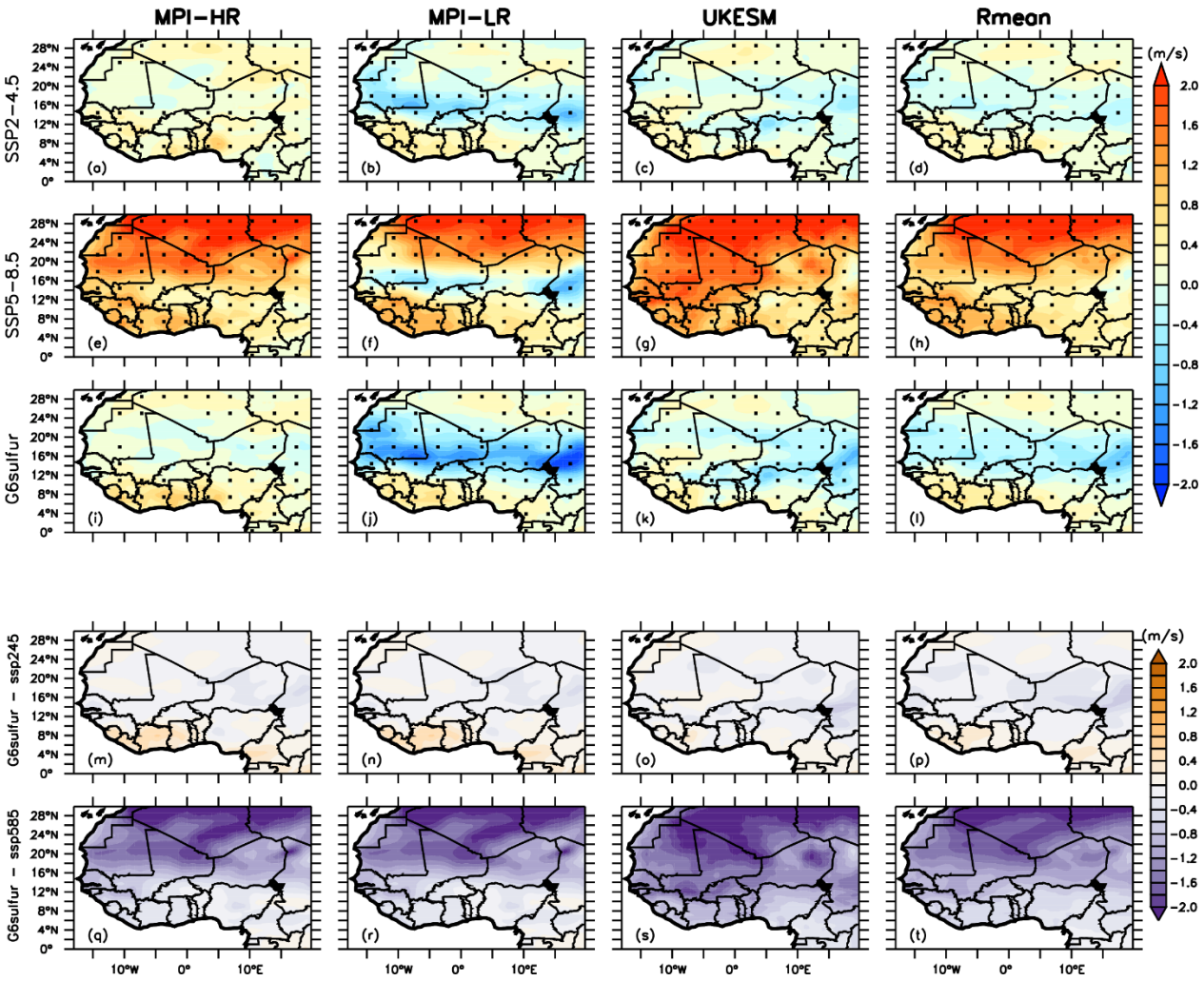

Figure 18 : Projected changes in annual mean wind speed in the far future (2070-2099) of the three models (MPI-HR, MPI-LR, UKESM) and their ensemble mean (Rmean) under SSP2-4.5 (a-d), SSP5-8.5 (e-h) and G6sulfur (i-l) scenarios, the difference between G6sulfur and SSP2-4.5 (m-p), the difference between G6sulfur and SSP5-8.5 (q-t). The dotted lines indicate areas that are significant at the 90 % level using the Student t-test.

Furthermore, the Rmean annual cycle projections for the different regions in West Africa show a significant decrease in temperature with the G6sulfur experiment (**Figure 19-b, e, h**). The Rmean project a slight decrease in wind speed with G6sulfur and almost similar to the SSP2-4.5 scenario (**Figure 19-c, f, i**). In contrast, G6sulfur increases solar irradiance in all regions of West Africa. But during the hot season (January-February-March-April-May) (**Figure 19-a, b, c**), G6sulfur decreases radiation and increases in the other seasons of the year. This may be due to high radiation during this warm season.

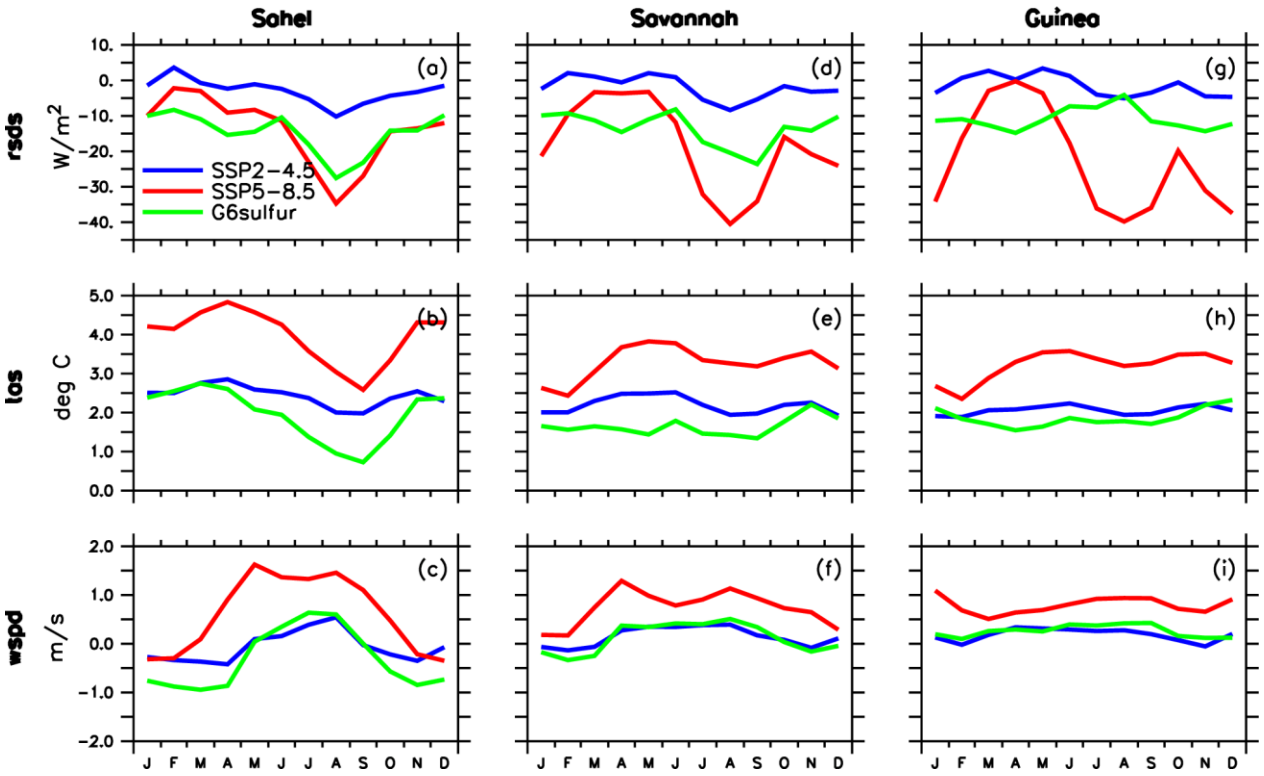

Figure 19 : Rmean projected changes in annual cycle of rsds, tas, and wspd over the three West African zones (Guinea, Savannah, and Sahel) in the far future (2070-2099) under SSP2-4.5, SSP5-8.5 and G6sulfur scenarios.

At the global scale (see Appendix; **Figures 31, 32, 33, 34, 35, and 36**), a decrease in temperature, solar irradiance and wind speed is projected with the G6sulfur experiment compared to the SSP5-8.5 scenario. However, in terms of solar irradiance we find that G6sulfur tends to increase radiation over West Africa, while a decrease is projected over South Africa, America, Australia. This could be explained by the parameterisation of the models with the G6sulphur experience. This is consistent with (Govindasamy and Caldeira, 2000) that aerosols in the stratosphere cannot cause a uniform decrease in radiation.

3.2.2. Projected changes in energy potential

Figures 20 and **21** exhibit the projected change in annual mean PVP and WPD, under the SSP2-4.5, SSP5-8.5, and G6sulfur scenarios over West Africa. The PVP shows a similarity feature to the radiation projection in **Figure 17**. The SSP5-8.5 projections decrease the PVP by about 4% and rise the WPD by 90 W/m^2 in the far future over West Africa. This decrease in PVP is due to a

reduction in surface irradiance and an increase in near-surface air temperature. In general, previous studies have shown that geoengineering could reduce the power of solar potential (Robock, 2008), (Robock, 2015), (Saeed et al., 2018). However, with the G6sulfur experiment used in our study, we find a 4% increase in PVP over the Gulf of Guinea and about 2% over the Sahel, and a 100 W/m^2 decrease in WPD over West Africa. On the other hand, we find a decrease in PVP at the global level, which is consistent with previous studies (see Appendix; **Figures 37,38**). The projected changes in the annual cycle of PV power potential and wind power density presented in **Figure 22** confirm the results found earlier. That is, G6sulfur tends to show a progressively increase PVP, while the SSP5-8.5 projections show a decrease in solar potential from the Sahel to the Gulf of Guinea. For the WPD projection, it is in the opposite direction to the PVP projection.

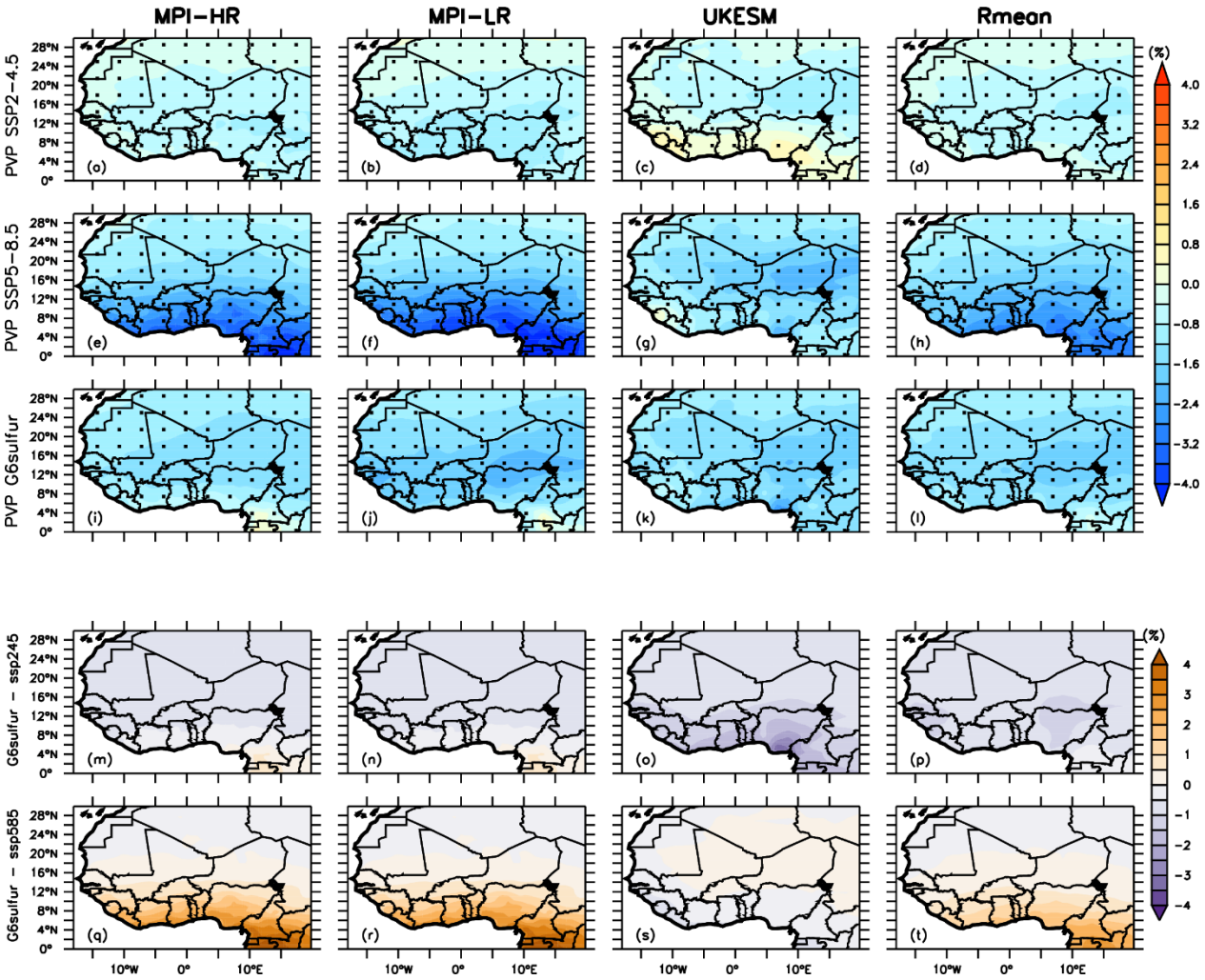

Figure 20 : Projected changes in annual mean PVP in the far future (2070-2099) of the three models (MPI-HR, MPI-LR, UKESM) and their ensemble mean (Rmean) under SSP2-4.5 (a-d),

SSP5-8.5 (e-h) and G6sulfur (i-l) scenarios, the difference between G6sulfur and SSP2-4.5 (m-p), the difference between G6sulfur and SSP5-8.5 (q-t). The dotted lines indicate areas that are significant at the 90 % level using the Student t-test.

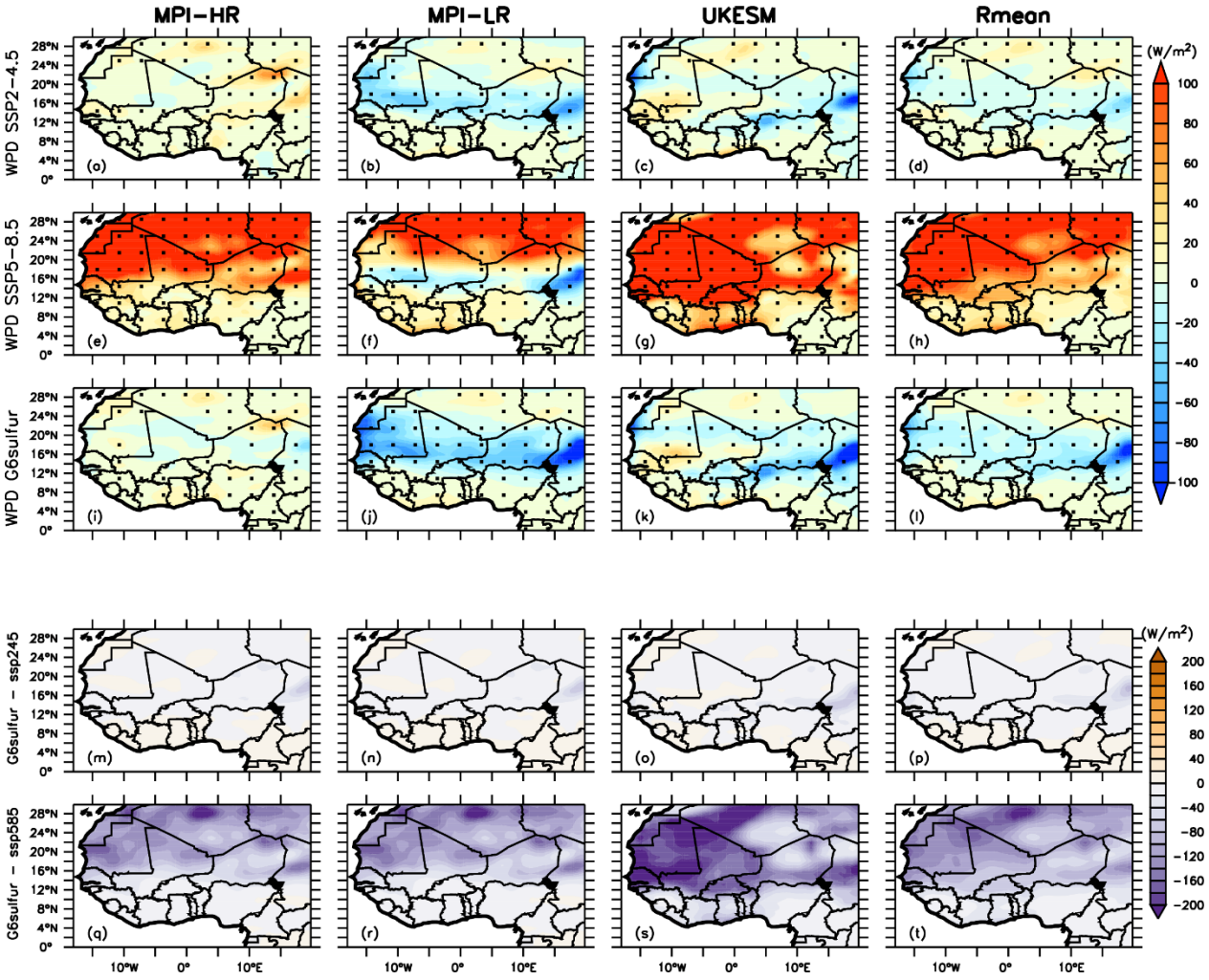

Figure 21: Projected changes in annual mean WPD in the far future (2070-2099) of the three models (MPI-HR, MPI-LR, UKESM) and their ensemble mean (Rmean) under SSP2-4.5 (a-d), SSP5-8.5 (e-h) and G6sulfur (i-l) scenarios, the difference between G6sulfur and SSP2-4.5 (m-p), the difference between G6sulfur and SSP5-8.5 (q-t). The dotted lines indicate areas that are significant at the 90 % level using the Student t-test.

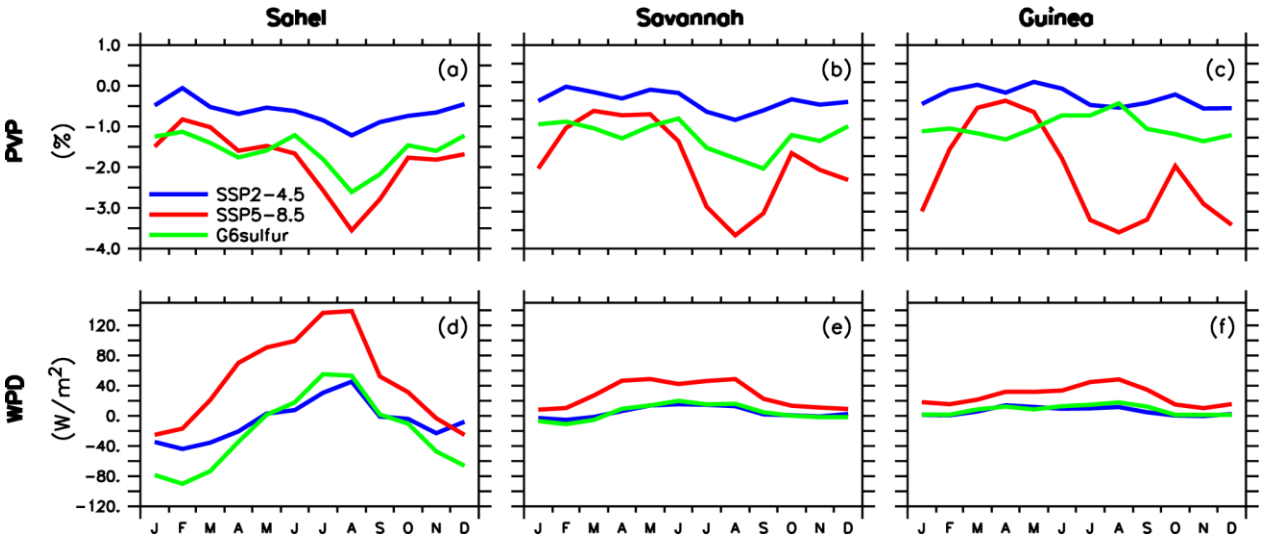

Figure 22 : Rmean projected changes in annual cycle of PVP and WPD over the three West Africa zones (Guinea, Savannah, and Sahel) in far future (2070-2099) under SSP2-4.5, SSP5-8.5 and G6sulfur scenarios.

In summary, **Figure 23** shows the projected changes in Rmean for temperature, solar irradiance, wind speed, PVP, and WPD in the far future (2070-2099) for each region of West Africa, which illustrates the effectiveness of G6sulfur in offsetting climate change. Using the interquartile range as a measure, the dispersion is calculated by the difference between the far future and the reference period of the Rmean.

The G6sulfur experiments show a strong temperature decrease in the Sahel, which decreases towards the Gulf of Guinea. In terms of projected changes in wind speed, G6sulfur also decreases wind speed compared to the SSP5-8.5 scenario, with a lager decrease in the Sahel than in the Guinean zone. Stratospheric sulfate aerosols are known to scatter solar radiation (shortwave, SW) and absorb near-infrared and longwave (LW) radiations. In our study, the G6sulfur experiment increases solar irradiance, resulting in increased PVP in different regions, but higher in the Gulf of Guinea, which contradicts the expected results of injecting sulfur particles into the atmosphere. The magnitudes observed with WPD are exceptionally low in the savannah and Guinea regions, showing a decrease, while in the Sahel, we expect high decrease with the G6sullfur scenario.

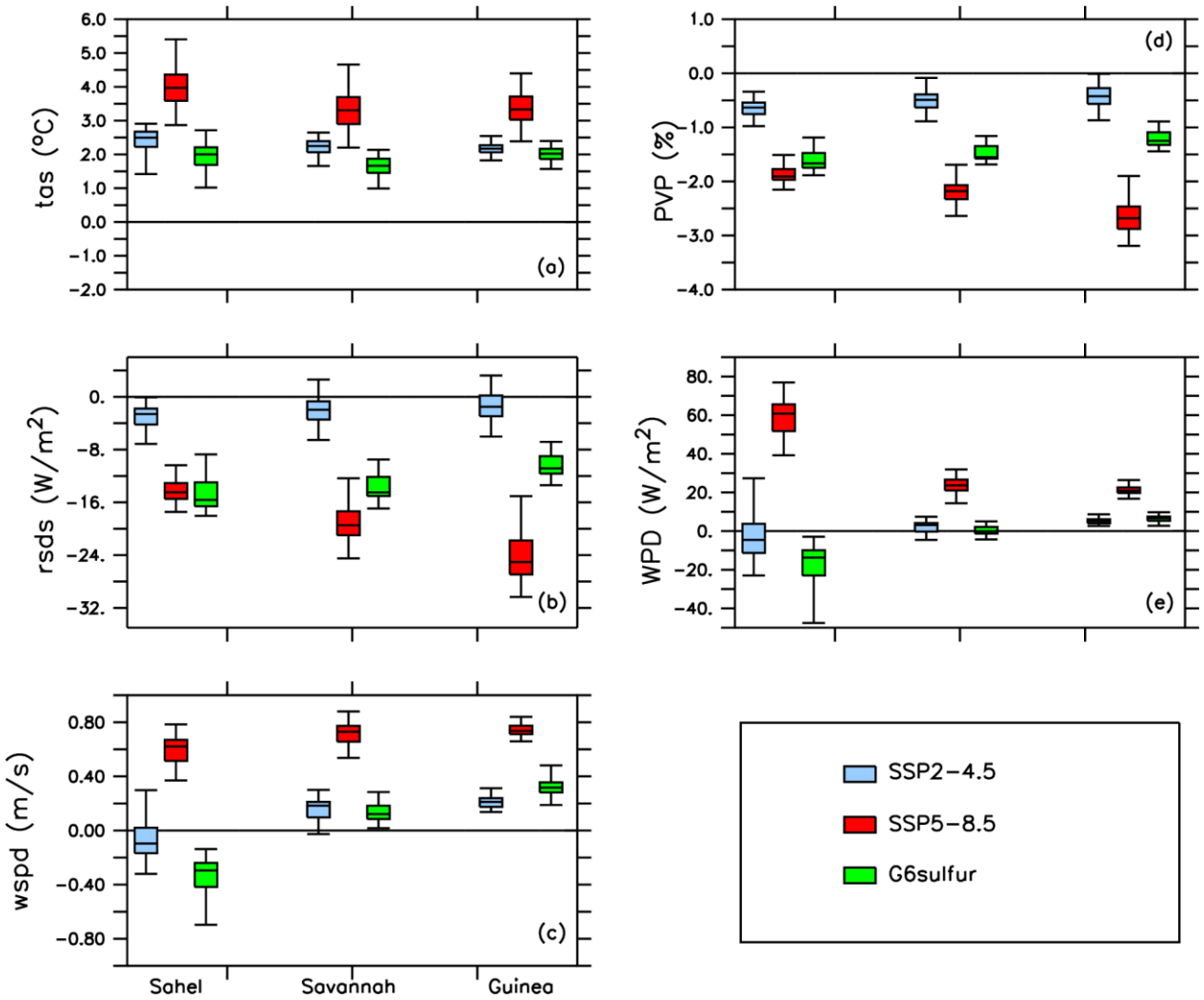

Figure 23 : Summary of projected changes in annual mean of temperature (tas), radiation (rsds), wind speed (wspd), PVP, and WPD over the three West African zones (Guinea, Savannah, and Sahel) in far future (2070-2099) under the SSP2-4.5, SSP5-8.5 and G6sulfur scenarios. Each boxplot indicates the minimum, first quartile, median, third quartile and maximum of the ensemble mean.

Conclusion and perspectives

This research highlights the potential impact of solar geoengineering on two renewable energy sources in West Africa. This study has tried to answer on how our energy resources would behave in the far future if any of the geoengineering methods were applied, especially the injection of sulfur particles into the atmosphere.

We analysed three models (MPI-HR, MPI-LR, UKESM) and their ensemble mean (Rmean) from CMIP6 and GeoMIP6 under climate scenarios SSP2-4.5 and SSP5-8.5, and G6sulfur experiment. These models were analysed for a current reference period (1985-2014) and for two future time slices, one short-term (2021-2050) and one long-term (2070-2099). We focused on the long-term projections because the changes were not significant in the short term. The ability of the simulations to reproduce the climate variables (i.e., solar irradiance, ambient air temperature, and surface wind speed) that affect the efficiency of the solar cells and the performance of wind turbine was assessed by comparing the model simulations with the observed data (ERA5). In agreement with observation, the simulations reproduced well the spatial pattern of climate variables, PVP, and WPD over West Africa, our first hypothesis is, therefore, confirmed.

The projected changes show that G6sulfur experiment exhibited a decrease in temperature and wind speed but, an increase in solar irradiance is projected over West Africa. In addition, PV potential increases and wind power density decreases with the G6sulfur experiment compared to the SSP5-8.5 scenarios. As these results are contrary to what we expect about the impact of solar geoengineering activities on PVP in West Africa, our second hypothesis is, therefore, not verified. As for the performance of the wind system, the impact of G6sulfur shows a decrease in WPD over West Africa, which is consistent with our expectation. Our third hypothesis is therefore confirmed. Our results are based on future projections of the G6sulfur scenario, which is one of the GeoMIP experiments. Thus, the results show the impacts that a solar geoengineering design could have in the future over West Africa.

For further research and conclusions from our study, it is therefore important to explore future perspectives, such as:

- The evaluation of other GeoMIP experiments like G6solar, which seeks to reduce the solar constant.
- The use of GLENS simulations that are performed with the Community Earth System

Model version 1 (CESM1), and which incorporates the Whole Atmosphere Community Climate Model as an atmospheric component and is fully coupled with the ocean, land, and sea ice models.

- Further study by examining the atmospheric components of the models used.

These perspectives will provide a comprehensive assessment of the inconsistency between observed and desired outcomes of geoengineering application. This will help policy makers better understand the risks of this new proposal to combat climate change.

Bibliography References

Abiodun, B. J., Adeyewa, Z. D., Oguntunde, P. G., Salami, A. T., & Ajayi, V. O. (2012). Modeling the impacts of reforestation on future climate in West Africa. *Theoretical and Applied Climatology*, *110*(1–2), 77–96. https://doi.org/10.1007/s00704-012-0614-1

Abiodun, B. J., Odoulami, R. C., Sawadogo, W., Oloniyo, O. A., Abatan, A. A., New, M., Lennard, C., Izidine, P., Egbebiyi, T. S., & MacMartin, D. G. (2021). Potential impacts of stratospheric aerosol injection on drought risk managements over major river basins in Africa. *Climatic Change*, *169*(3–4), 1–19. https://doi.org/10.1007/s10584-021-03268-w

Akinsanola, A. A., Ogunjobi, K. O., Abolude, A. T., & Salack, S. (2021a). Projected changes in wind speed and wind energy potential over West Africa in CMIP6 models. *Environmental Research Letters*, *16*(4). https://doi.org/10.1088/1748-9326/abed7a

Akinsanola, A. A., Ogunjobi, K. O., Abolude, A. T., & Salack, S. (2021b). *Projected changes in wind speed and wind energy potential over West Africa in CMIP6 models OPEN ACCESS Projected changes in wind speed and wind energy potential over West Africa in CMIP6 models*.

Alamou, E. A., Zandagba, J. E., Biao, E. I., Obada, E., Da-Allada, C. Y., Bonou, F. K., Pomalegni, Y., Baloitcha, E., Tilmes, S., & Irvine, P. J. (2022). Impact of Stratospheric Aerosol Geoengineering on Extreme Precipitation and Temperature Indices in West Africa Using GLENS Simulations. *Journal of Geophysical Research: Atmospheres*, *127*(9). https://doi.org/10.1029/2021JD035855

Caldeira, K., Bala, G., & Cao, L. (2013). The science of geoengineering. *Annual Review of Earth and Planetary Sciences*, *41*, 231–256. https://doi.org/10.1146/annurev-earth-042711-105548

Chen, G., Wang, W.-C., Bao, Q., & Li, J. (2022). Evaluation of simulated cloud diurnal variation in CMIP6 climate models. *Journal of Geophysical Research: Atmospheres*, 127, e2021JD036422. https://doi.org/10.1029/2021JD036422

Crutzen, P. J. (2006). Albedo enhancement by stratospheric sulfur injections: A contribution to resolve a policy dilemma? *Climatic Change*, *77*(3–4), 211–220. https://doi.org/10.1007/s10584-006-9101-y

Da-Allada, C. Y., Baloïtcha, E., Alamou, E. A., Awo, F. M., Bonou, F., Pomalegni, Y., Biao, E. I., Obada, E., Zandagba, J. E., Tilmes, S., & Irvine, P. J. (2020). Changes in West African

Summer Monsoon Precipitation Under Stratospheric Aerosol Geoengineering. *Earth's Future*, *8*(7), 1–13. https://doi.org/10.1029/2020EF001595

Dos Anjos, P. S., Alves Da Silva, A. S., Stošić, B., & Stošić, T. (2015). Long-term correlations and cross-correlations in wind speed and solar radiation temporal series from Fernando de Noronha Island, Brazil. *Physica A: Statistical Mechanics and Its Applications*, *424*, 90–96. https://doi.org/10.1016/j.physa.2015.01.003

Dullaart, J. C. M., Muis, S., Bloemendaal, N., & Aerts, J. C. J. H. (2020). Advancing global storm surge modelling using the new ERA5 climate reanalysis. *Climate Dynamics*, *54*(1–2), 1007–1021. https://doi.org/10.1007/s00382-019-05044-0

Ellabban, O., Abu-Rub, H., & Blaabjerg, F. (2014). Renewable energy resources: Current status, future prospects and their enabling technology. *Renewable and Sustainable Energy Reviews*, *39*, 748–764. https://doi.org/10.1016/j.rser.2014.07.113

ETC Group. (2014). Geoengineering and Climate Change Implications for Africa. *ETC Group*. https://www.etcgroup.org/sites/www.etcgroup.org/files/geoengineering-africa-etc-2014.pdf

Eyring, V., Bony, S., Meehl, G. A., Senior, C. A., Stevens, B., Stouffer, R. J., & Taylor, K. E. (2016). Overview of the Coupled Model Intercomparison Project Phase 6 (CMIP6) experimental design and organization. *Geoscientific Model Development*, *9*(5), 1937–1958. https://doi.org/10.5194/gmd-9-1937-2016

Govindasamy, B., & Caldeira, K. (2000). Geoengineering Earth's radiation balance to mitigate CO2-induced climate change. *Geophysical Research Letters*, *27*(14), 2141–2144. https://doi.org/10.1029/1999GL006086

Guerri, A. B. O. (2012). *Influence de la rugosité sur les caractéristiques aérodynamiques d ' un profil de pale d ' éolienne*. *15*, 235–247.

Heckendorn, P., Weisenstein, D., Fueglistaler, S., Luo, B. P., Rozanov, E., Schraner, M., Thomason, L. W., & Peter, T. (2009). The impact of geoengineering aerosols on stratospheric temperature and ozone. *Environmental Research Letters*, *4*(4). https://doi.org/10.1088/1748-9326/4/4/045108

Hersbach, H., Bell, B., Berrisford, P., Horányi, A., Sabater, J. M., Nicolas, J., Radu, R., Schepers, D., Simmons, A., Soci, C., & Dee, D. (2019). Global reanalysis: goodbye ERA-Interim, hello ERA5. *ECMWF Newsletter*, *159*, 17–24. https://doi.org/10.21957/vf291hehd7

IPCC. (2021). Climate Change 2021: The Physical Science Basis. Contribution of Working

Group I to the Sixth Assessment Report of the Intergovernmental Panel on Climate Change [Masson-Delmotte, V., P. Zhai, A. Pirani, S. L. Connors, C. Péan, S. Berger, N. Caud, Y. Chen,. *Cambridge University Press, In Press*, 3949. https://www.ipcc.ch/report/ar6/wg1/downloads/report/IPCC_AR6_WGI_Full_Report.pdf

Jerez, S., Tobin, I., Vautard, R., Montávez, J. P., López-Romero, J. M., Thais, F., Bartok, B., Christensen, O. B., Colette, A., Déqué, M., Nikulin, G., Kotlarski, S., Van Meijgaard, E., Teichmann, C., & Wild, M. (2015). The impact of climate change on photovoltaic power generation in Europe. *Nature Communications*, *6*. https://doi.org/10.1038/ncomms10014

Jones, A. (2019). MOHC UKESM1.0-LL model output prepared for CMIP6 GeoMIP G6sulfur. Earth System Grid Federation. https://doi.org/10.22033/ESGF/CMIP6.5822

Junclaus, J., et al. (2019). MPI-M MPIESM1.2-HR model output prepared for CMIP6 CMIP. Earth System Grid Federation. https://doi.org/10.22033/ESGF/CMIP6.741

Kaito, C., Ito, A., Kimura, S., Kimura, Y., Saito, Y., & Nakada, T. (2000). Topotactical growth of indium sulfide by evaporation of metal onto molybdenite. In *Journal of Crystal Growth* (Vol. 218, Issue 2). https://doi.org/10.1016/S0022-0248(00)00575-3

Kalidindi, S., Bala, G., Modak, A., & Caldeira, K. (2015). Modeling of solar radiation management: a comparison of simulations using reduced solar constant and stratospheric sulphate aerosols. *Climate Dynamics*, *44*(9–10), 2909–2925. https://doi.org/10.1007/s00382-014-2240-3

Karami, K., Tilmes, S., Muri, H., & Mousavi, S. V. (2020). Storm Track Changes in the Middle East and North Africa Under Stratospheric Aerosol Geoengineering. *Geophysical Research Letters*, *47*(14). https://doi.org/10.1029/2020GL086954

Keith, D. W. (2000). *GEOENGINEERING THE CLIMATE: History and Prospect 1*. www.annualreviews.org

Kravitz, B., Robock, A., Tilmes, S., Boucher, O., English, J. M., Irvine, P. J., Jones, A., Lawrence, M. G., MacCracken, M., Muri, H., Moore, J. C., Niemeier, U., Phipps, S. J., Sillmann, J., Storelvmo, T., Wang, H., & Watanabe, S. (2015). The Geoengineering Model Intercomparison Project Phase 6 (GeoMIP6): Simulation design and preliminary results. *Geoscientific Model Development*, *8*(10), 3379–3392. https://doi.org/10.5194/gmd-8-3379-2015

Kuswanto, H., Kravitz, | Ben, Miftahurrohmah, B., Fauzi, F., Sopahaluwaken, A., & Moore, J.

(2021). *Impact of solar geoengineering on temperatures over the Indonesian Maritime Continent*. https://doi.org/10.1002/joc.7391

Lhomme, P., Michez, D., Christmann, S., Scheuchl, E., Abdouni, I. El, Hamroud, L., Ihsane, O., Sentil, A., Smaili, M. C., Schwarz, M., Dathe, H. H., Straka, J., Pauly, A., Schmid-Egger, C., Patiny, S., Terzo, M., Müller, A., Praz, C., Risch, S., … Rasmont, P. (2020). The wild bees (Hymenoptera: Apoidea) of Morocco. In *Zootaxa* (Vol. 4892, Issue 1). https://doi.org/10.11646/zootaxa.4892.1.1

Mann, I. R., O'Brien, T. P., & Milling, D. K. (2004). Correlations between ULF wave power, solar wind speed, and relativistic electron flux in the magnetosphere: Solar cycle dependence. *Journal of Atmospheric and Solar-Terrestrial Physics*, *66*(2), 187–198. https://doi.org/10.1016/j.jastp.2003.10.002

Mavromatakis, F., Makrides, G., Georghiou, G., Pothrakis, A., Franghiadakis, Y., Drakakis, E., & Koudoumas, E. (2010). Modeling the photovoltaic potential of a site. *Renewable Energy*, *35*(7), 1387–1390. https://doi.org/10.1016/j.renene.2009.11.010

Niemeier, U., et al. (2019a). MPI-M MPI-ESM1.2-HR model output prepared for CMIP6 GeoMIP G6sulfur. Earth System Grid Federation. https://doi.org/10.22033/ESGF/CMIP6.15300

Niemeier, U., et al. (2019b). MPI-M MPI-ESM1.2-LR model output prepared for CMIP6 GeoMIP G6sulfur. Earth System Grid Federation. https://doi.org/10.22033/ESGF/CMIP6.6448

Niemeier, U., H. Richter, J., & Tilmes, S. (2020). Differing responses of the quasi-biennial oscillation to artificial SO2 injections in two global models. *Atmospheric Chemistry and Physics*, *20*(14), 8975–8987. https://doi.org/10.5194/acp-20-8975-2020

Niemeier, U., & Schmidt, H. (2017). Changing transport processes in the stratosphere by radiative heating of sulfate aerosols. *Atmospheric Chemistry and Physics*, *17*(24), 14871–14886. https://doi.org/10.5194/acp-17-14871-2017

Nowack, P. J., Abraham, N. L., Braesicke, P., & Pyle, J. A. (2016). Stratospheric ozone changes under solar geoengineering: Implications for UV exposure and air quality. *Atmospheric Chemistry and Physics*, *16*(6), 4191–4203. https://doi.org/10.5194/acp-16-4191-2016

Panwar, N. L., Kaushik, S. C., & Kothari, S. (2011). Role of renewable energy sources in environmental protection: A review. *Renewable and Sustainable Energy Reviews*, *15*(3), 1513–1524. https://doi.org/10.1016/j.rser.2010.11.037

Pinto, I., Jack, C., Lennard, C., Tilmes, S., & Odoulami, R. C. (2020). Africa's Climate Response

to Solar Radiation Management With Stratospheric Aerosol. *Geophysical Research Letters*, *47*(2), 1–10. https://doi.org/10.1029/2019GL086047

Robock, A. (2008). 20 Reasons Why Geoengineering May Be a Bad Idea. *Bulletin of the Atomic Scientists*, *64*(2), 14–18. https://doi.org/10.2968/064002006

Robock, A. (2015). Stratospheric aerosol geoengineering. *AIP Conference Proceedings*, *1652*(Pse Iii), 183–197. https://doi.org/10.1063/1.4916181

Russell, L. M., Rasch, P. J., MacE, G. M., Jackson, R. B., Shepherd, J., Liss, P., Leinen, M., Schimel, D., Vaughan, N. E., Janetos, A. C., Boyd, P. W., Norby, R. J., Caldeira, K., Merikanto, J., Artaxo, P., Melillo, J., & Morgan, M. G. (2012). Ecosystem impacts of geoengineering: A review for developing a science plan. *Ambio*, *41*(4), 350–369. https://doi.org/10.1007/s13280-012-0258-5

Saeed, F., Schleussner, C.-F., & Hare, W. (2018). Why geoengineering is not a solution to the climate problem. *Climate Analytics*, 1–8.

Sawadogo, W., Abiodun, B. J., & Okogbue, E. C. (2019). Projected changes in wind energy potential over West Africa under the global warming of 1.5 °C and above. *Theoretical and Applied Climatology*, *138*(1–2), 321–333. https://doi.org/10.1007/s00704-019-02826-8

Sawadogo, W., Abiodun, B. J., & Okogbue, E. C. (2020). Impacts of global warming on photovoltaic power generation over West Africa. *Renewable Energy*, *151*, 263–277. https://doi.org/10.1016/j.renene.2019.11.032

Sawadogo, W., Simões, M., Aissatou, R., & Rosmeri, F. (2021). Current and future potential of solar and wind energy over Africa using the RegCM4 CORDEX - CORE ensemble. *Climate Dynamics*, *57*(5), 1647–1672. https://doi.org/10.1007/s00382-020-05377-1

Schupfer, M., et al. (2021). DKRZ MPI-ESM1.2-LR model output prepared for CMIP6 ScenarioMIP. Earth System Grid Federation. https://doi.org/10.22033/ESGF/CMIP6.15349

Sellar, A. A., Jones, C. G., Mulcahy, J. P., Tang, Y., Yool, A., Wiltshire, A., O'Connor, F. M., Stringer, M., Hill, R., Palmieri, J., Woodward, S., de Mora, L., Kuhlbrodt, T., Rumbold, S. T., Kelley, D. I., Ellis, R., Johnson, C. E., Walton, J., Abraham, N. L., … Zerroukat, M. (2019). UKESM1: Description and Evaluation of the U.K. Earth System Model. *Journal of Advances in Modeling Earth Systems*, *11*(12), 4513–4558. https://doi.org/10.1029/2019MS001739

Simão, M. L., Videiro, P. M., Silva, P. B. A., de Freitas Assad, L. P., & Sagrilo, L. V. S. (2020).

Application of Taylor diagram in the evaluation of joint environmental distributions' performances. *Marine Systems and Ocean Technology*, *15*(3), 151–159. https://doi.org/10.1007/s40868-020-00081-5

Tang, Y., Rumbold, S., Ellis, R., Kelley, D., Mulcahy, J., Sellar, A., Walton, J., Jones, C. (2019). MOHC UKESM1.0-LL model output prepared for CMIP6 CMIP.Earth System Grid Federation. https://doi.org/10.22033/ESGF/CMIP6.1569

The Royal Society. (2009). Geoengineering the climate: science, governance and uncertainty. In *Clean Technologies and Environmental Policy* (Issue September).

Tilmes, S., Visioni, D., Jones, A., Haywood, J., Séférian, R., Nabat, P., Boucher, O., Bednarz, E. M., & Niemeier, U. (2021). Stratospheric Ozone Response to Sulfate Aerosol and Solar Dimming Climate Interventions based on the G6 Geoengineering Model Intercomparison Project (GeoMIP) Simulations. *Atmospheric Chemistry and Physics Discussions*, *December*, 1–31. https://doi.org/10.5194/acp-2021-1003

Turner, R. E., Bernier, J. C., Barras, J. a, Ferina, N. F., Zhang, X., Sheremet, A., Cahoon, D. R., Nichols, L. G., Wright, M., Rouge, B., Nyman, J. a, Delaune, R. D., Roberts, H. H., Patrick, W. H., Swenson, E. M., Milan, C. S., Weinstein, M., Kreeger, D. a, Chakrapani, G. J., … Oswald, T. a. (2010). A Combined Mitigation / Geoengineering. *Changes*, *October 2006*, 452–454.

Visioni, D., Macmartin, D. G., Kravitz, B., Boucher, O., Jones, A., Lurton, T., Martine, M., Mills, M. J., Nabat, P., Niemeier, U., Séférian, R., & Tilmes, S. (2021). Identifying the sources of uncertainty in climate model simulations of solar radiation modification with the G6sulfur and G6solar Geoengineering Model Intercomparison Project (GeoMIP) simulations. *Atmospheric Chemistry and Physics*, *21*(13), 10039–10063. https://doi.org/10.5194/acp-21-10039-2021

Yu, K. M. K., Curcic, I., Gabriel, J., & Tsang, S. C. E. (2008). Recent advances in CO2 capture and utilization. *ChemSusChem*, *1*(11), 893–899. https://doi.org/10.1002/cssc.200800169

Zarnetske, P. L., Gurevitch, J., Franklin, J., Groffman, P. M., Harrison, C. S., Hellmann, J. J., Hoffman, F. M., Kothari, S., Robock, A., Tilmes, S., Visioni, D., Wu, J., Xia, L., & Yang, C. E. (2021). Potential ecological impacts of climate intervention by reflecting sunlight to cool Earth. *Proceedings of the National Academy of Sciences of the United States of America*, *118*(15). https://doi.org/10.1073/PNAS.1921854118

Appendix

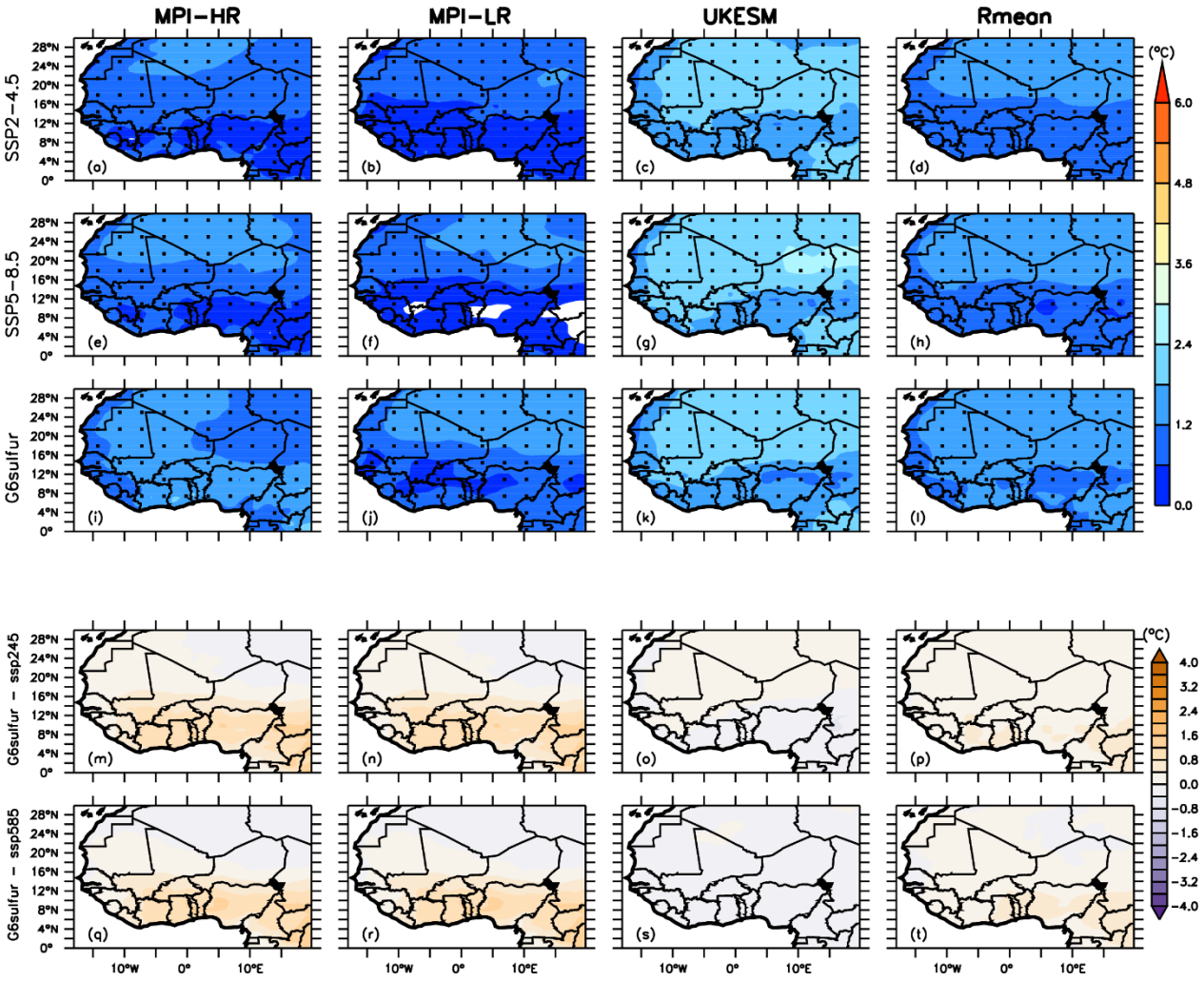

Figure 24 : Projected changes in annual mean of temperature in the near future (2021-2050) of the three models (MPI-HR, MPI-LR, UKESM) and their ensemble mean (Rmean) under SSP2-4.5 (a-d), SSP5-8.5 (e-h) and G6sulfur (i-l) scenarios over West Africa. The dotted lines indicate areas that are significant at the 90 % level using the Student t-test.

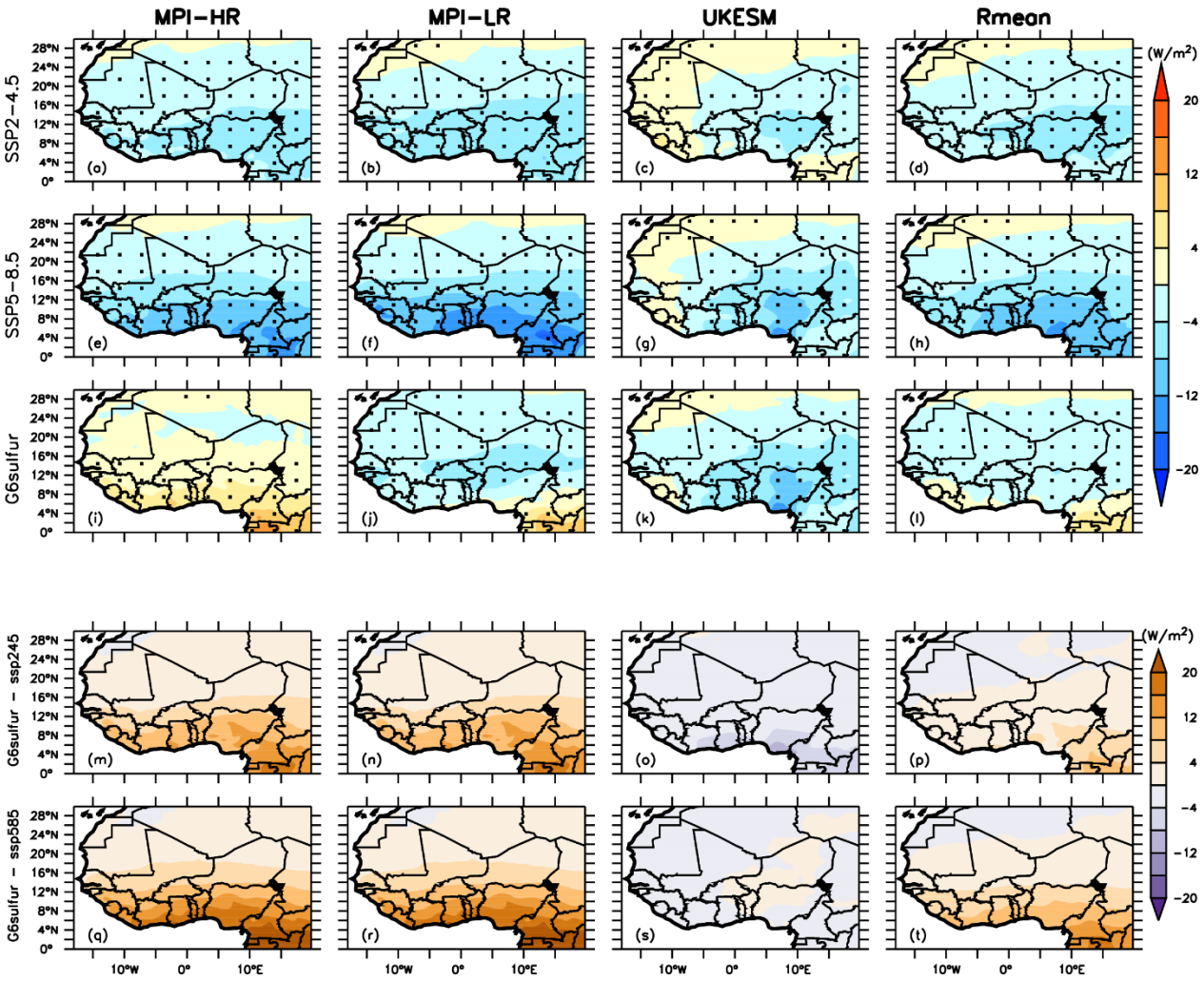

Figure 25 : Same as Figure.24, but for solar irradiance.

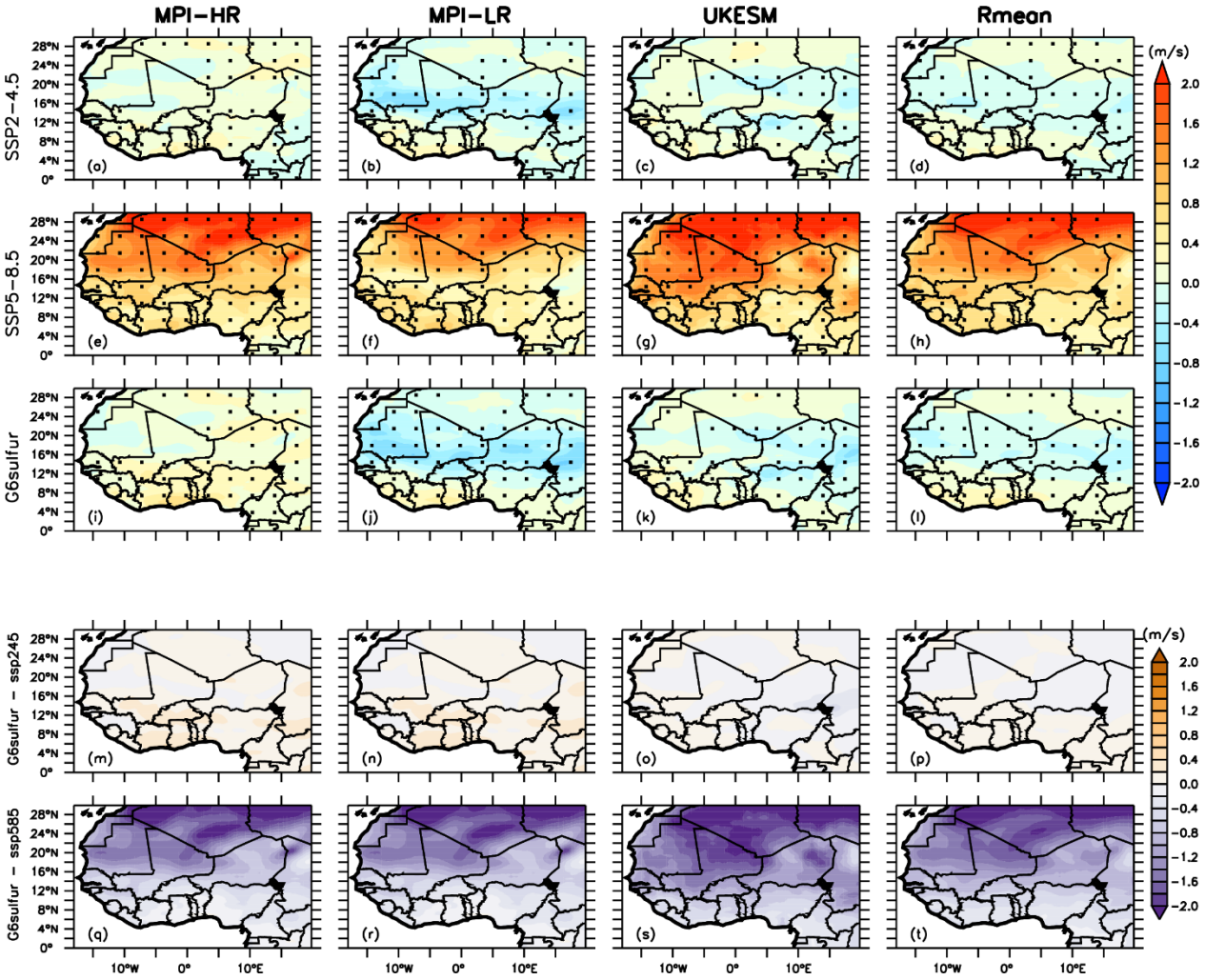

Figure 26 : Same as Figure.24, but for wind speed.

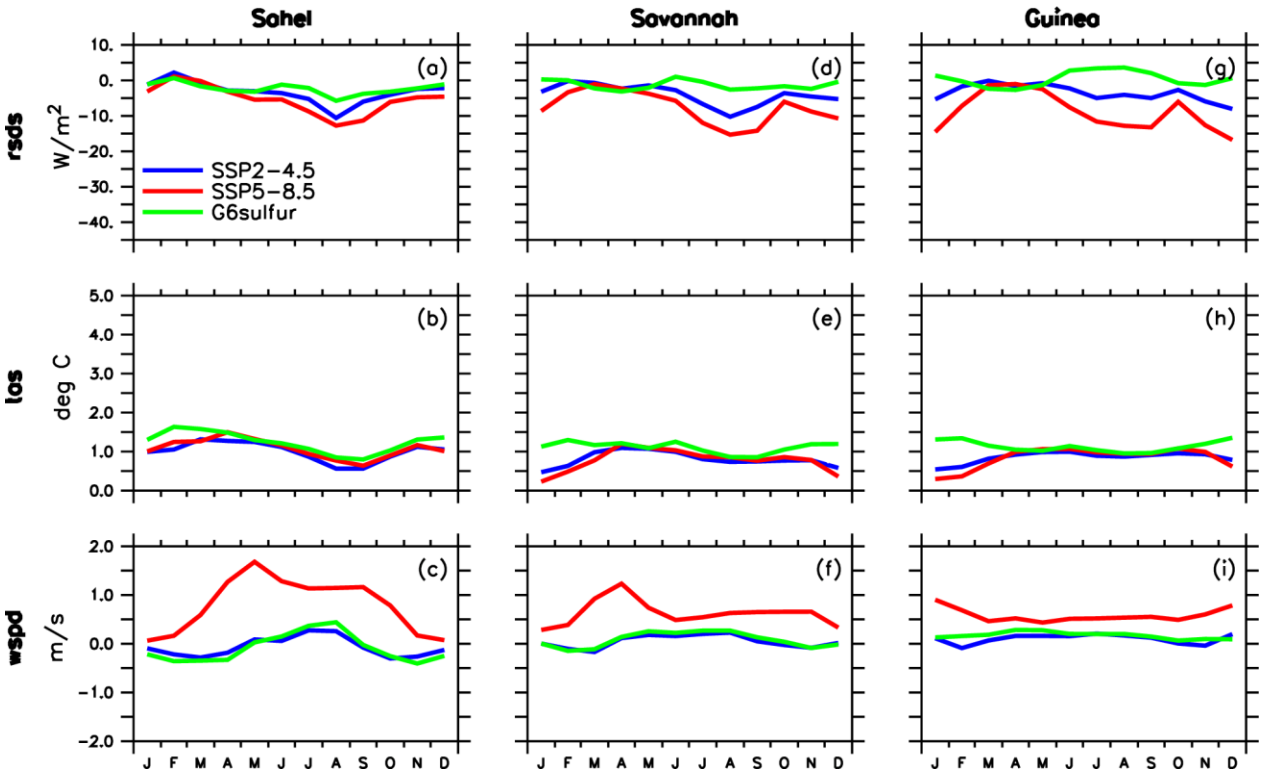

Figure 27 : Rmean projected changes in annual cycle of rsds, tas, and wspd over the three West Africa zones (Guinea, Savannah, and Sahel) in the near future (2021-2050) under SSP2-4.5, SSP5-8.5 and G6sulfur scenarios.

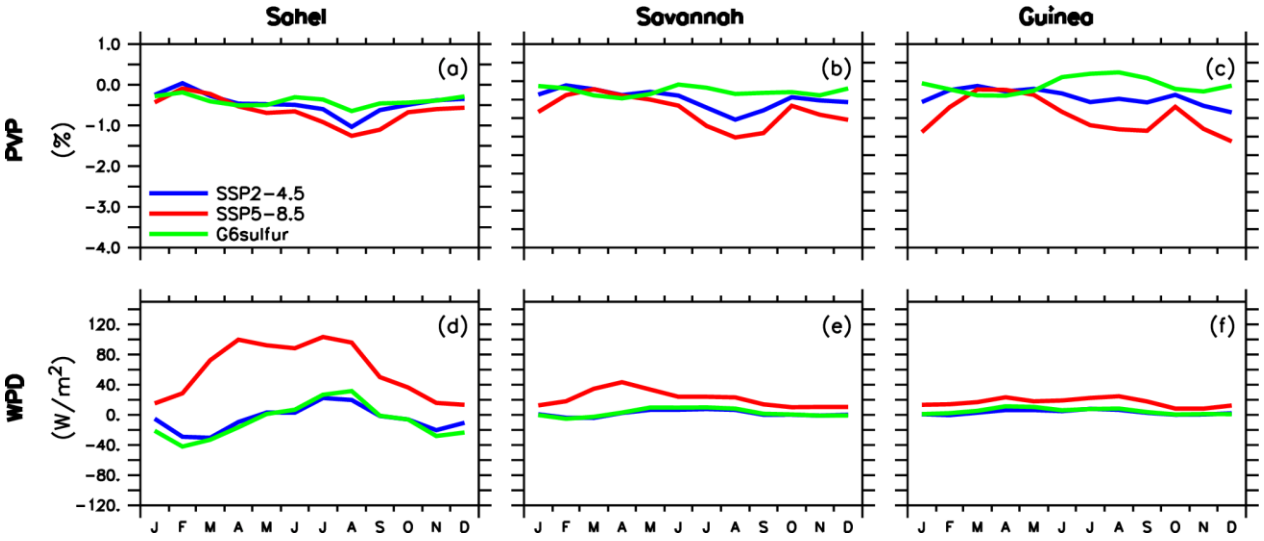

Figure 28 : Rmean projected changes in annual cycle of photovoltaic power potential (PVP) and wind power density (WPD) over the three West Africa zones (Guinea, Savannah, and Sahel) in the near future (2021-2050) under SSP2-4.5, SSP5-8.5 and G6sulfur scenarios.

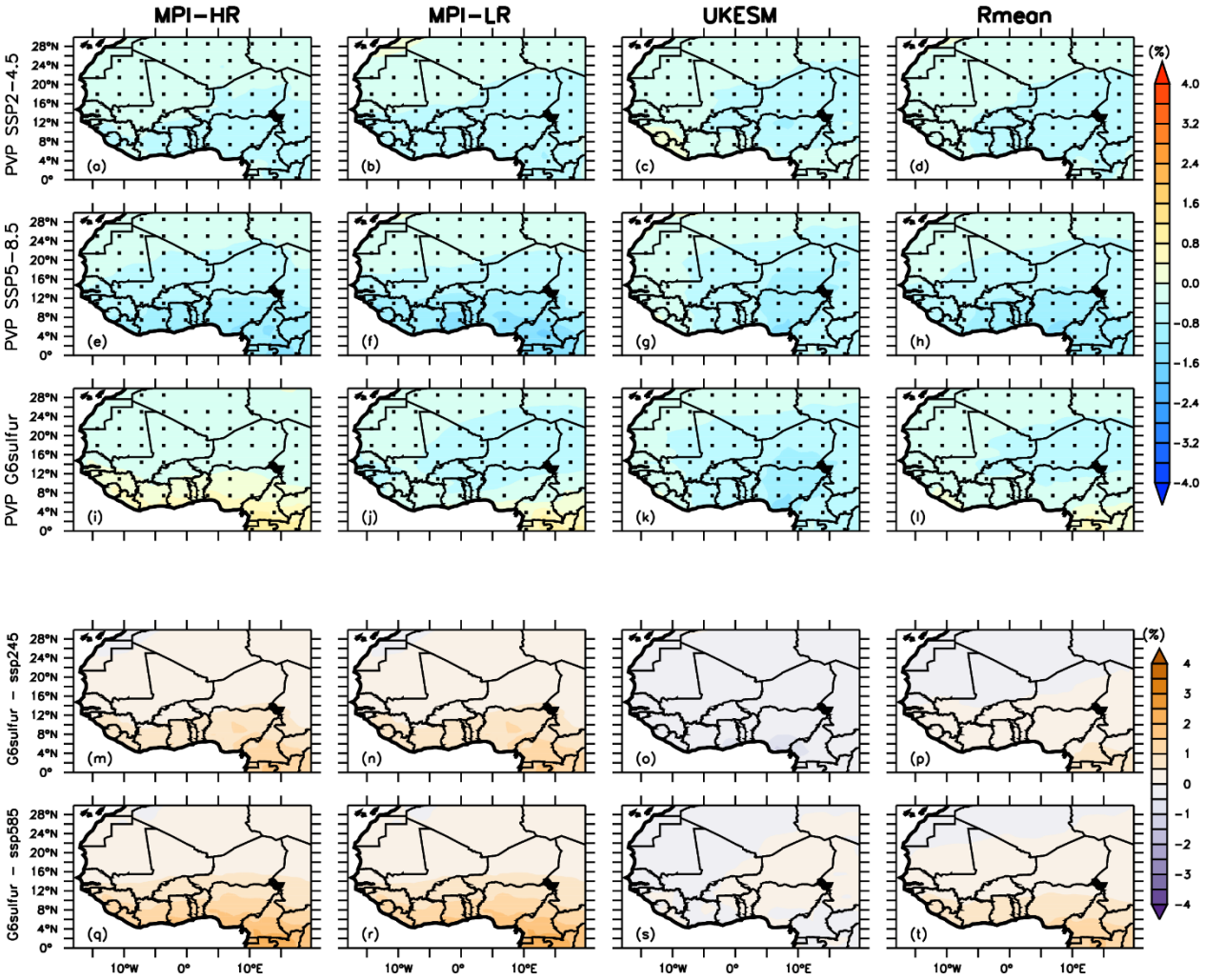

Figure 29 : Same as Figure.24, but for photovoltaic power potential (PVP).

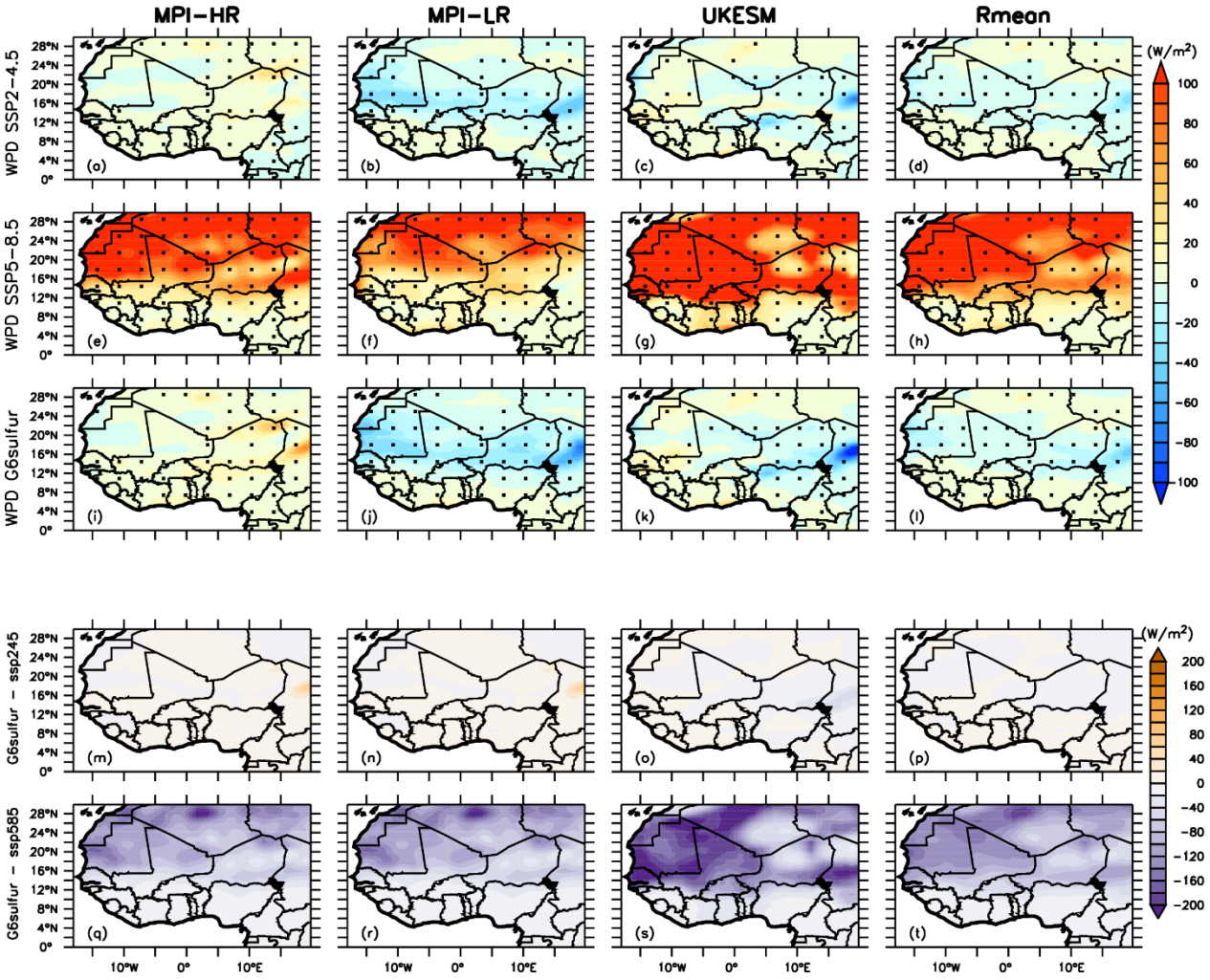

Figure 30 : Same as Figure.24, but for wind power density (WPD).

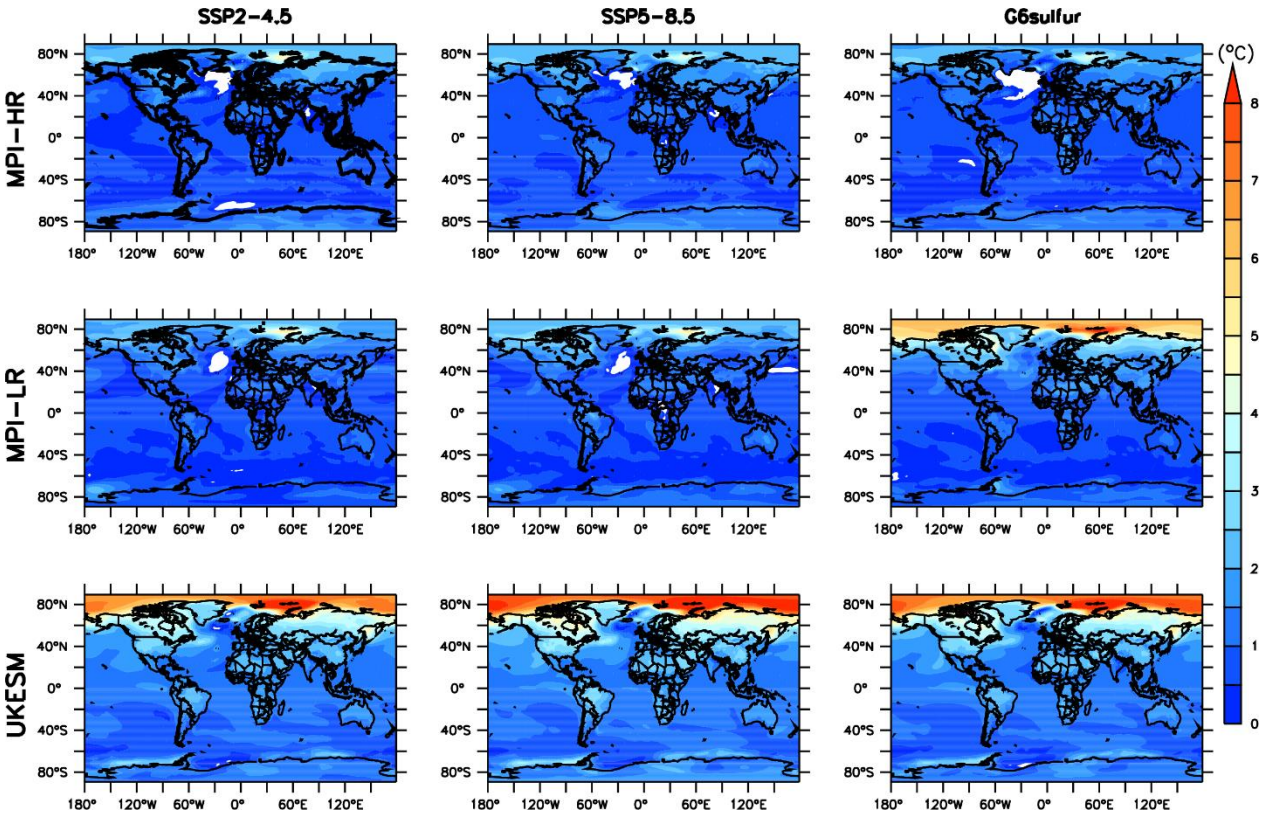

Figure 31 : Global mean of temperature changes projected in the near future (2021-2050) of the three models (MPI-HR, MPI-LR, UKESM) under SSP2-4.5, SSP5-8.5, and G6sulfur scenarios.

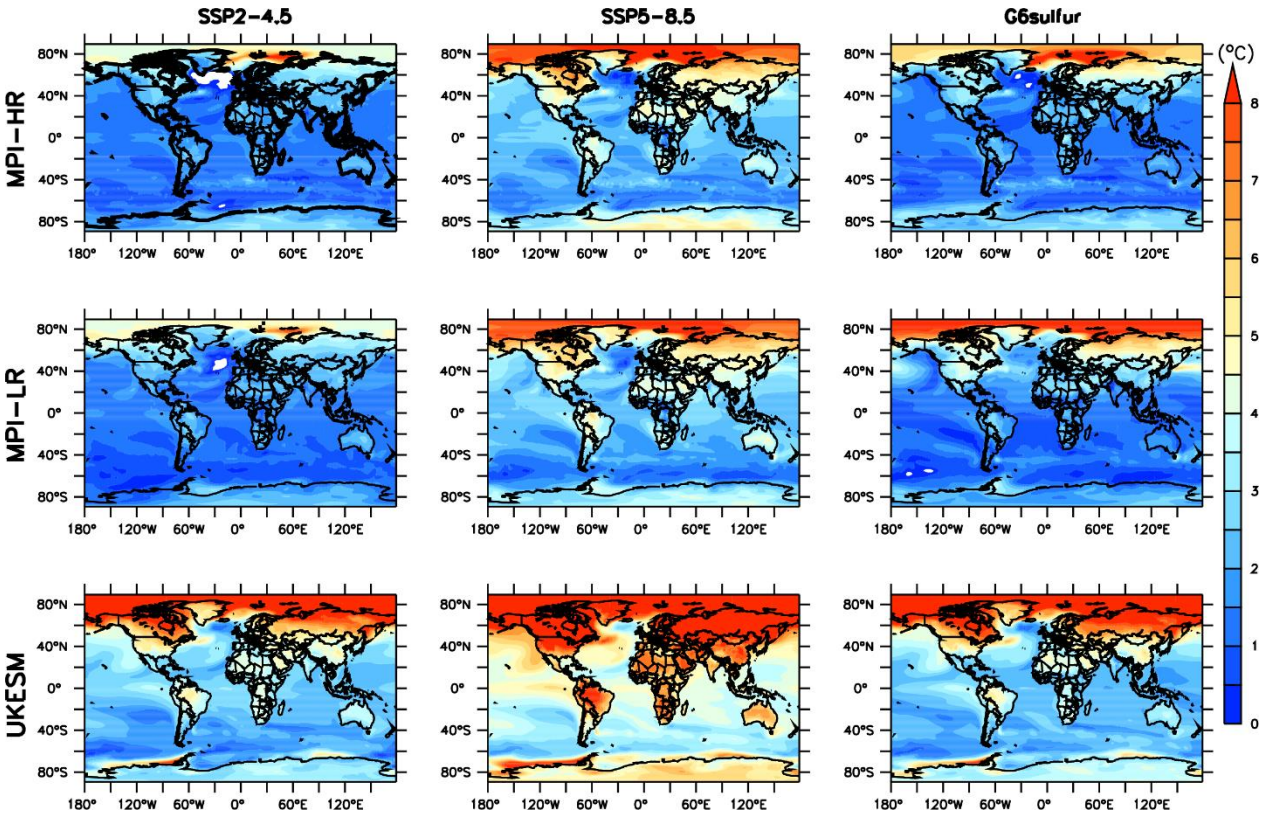

Figure 32 : Same as Figure.31, but in the far future (2070-2099)

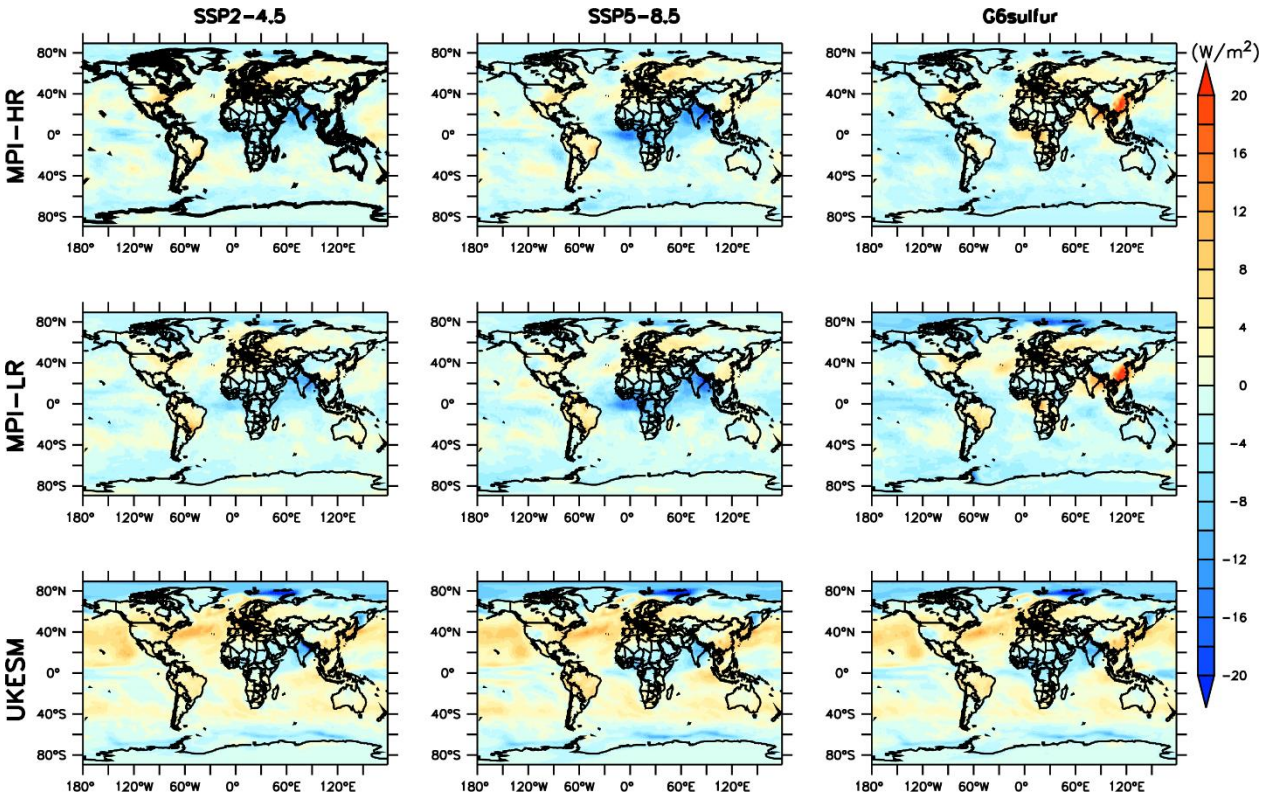

Figure 33 : Global mean of radiation changes projected in the near future (2021-2050) of the three models (MPI-HR, MPI-LR, UKESM) under SSP2-4.5, SSP5-8.5, and G6sulfur scenarios.

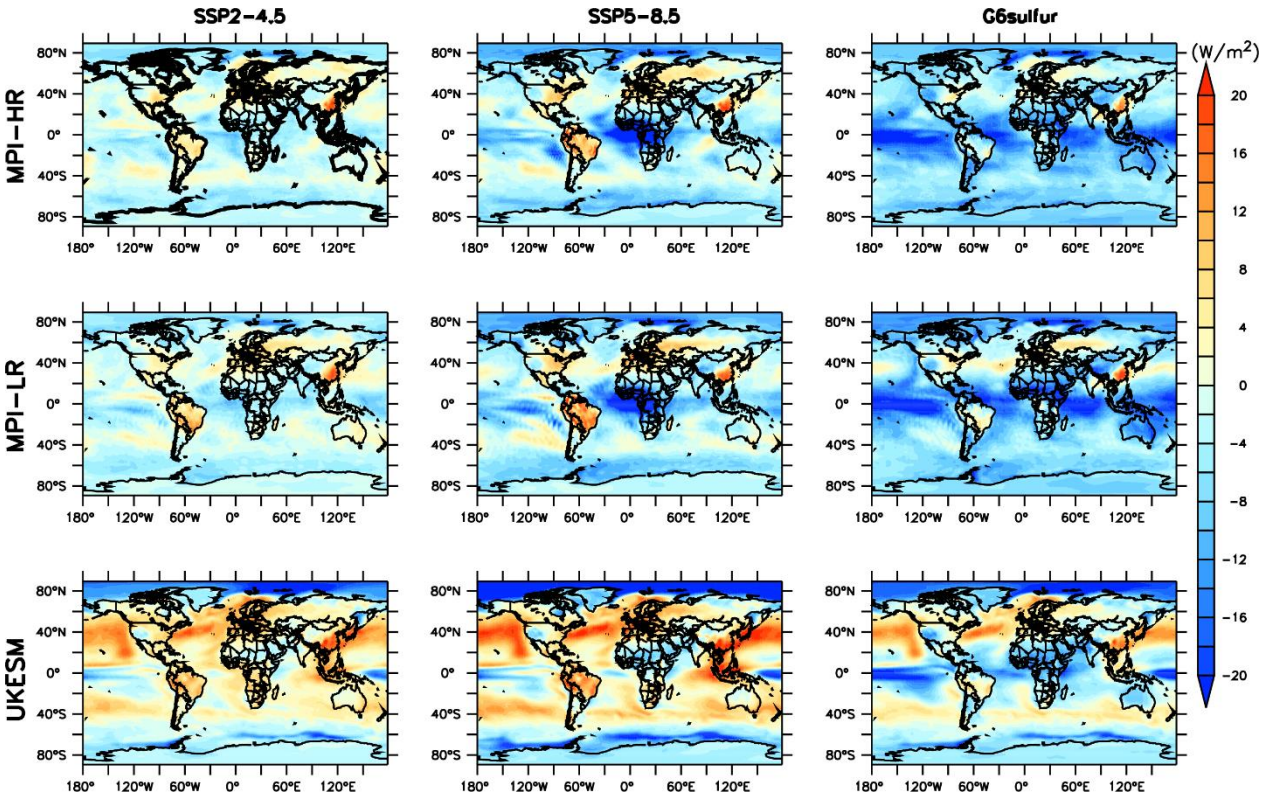

Figure 34 : Same as Figure.33, but in the far future (2070-2099)

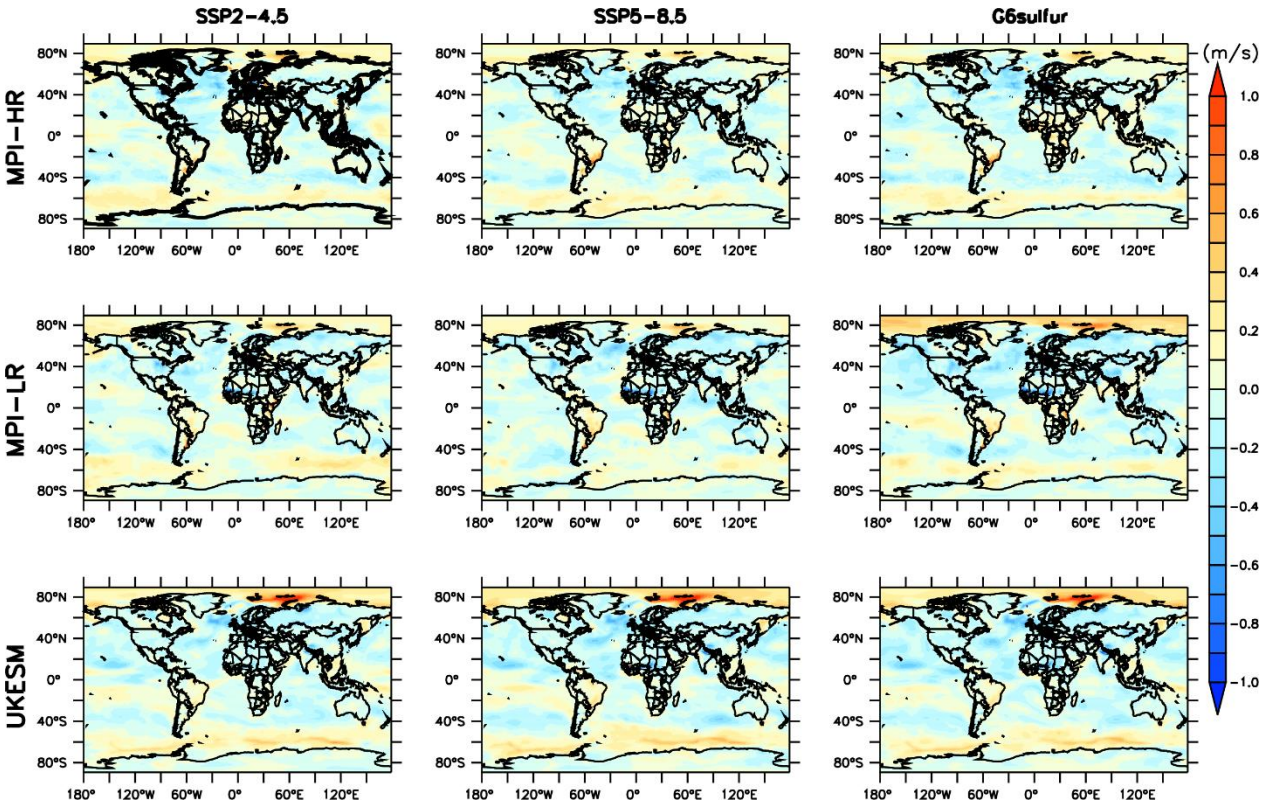

Figure 35 : Global mean of wind speed changes projected in the near future (2021-2050) of the three models (MPI-HR, MPI-LR, UKESM) under SSP2-4.5, SSP5-8.5, and G6sulfur scenarios.

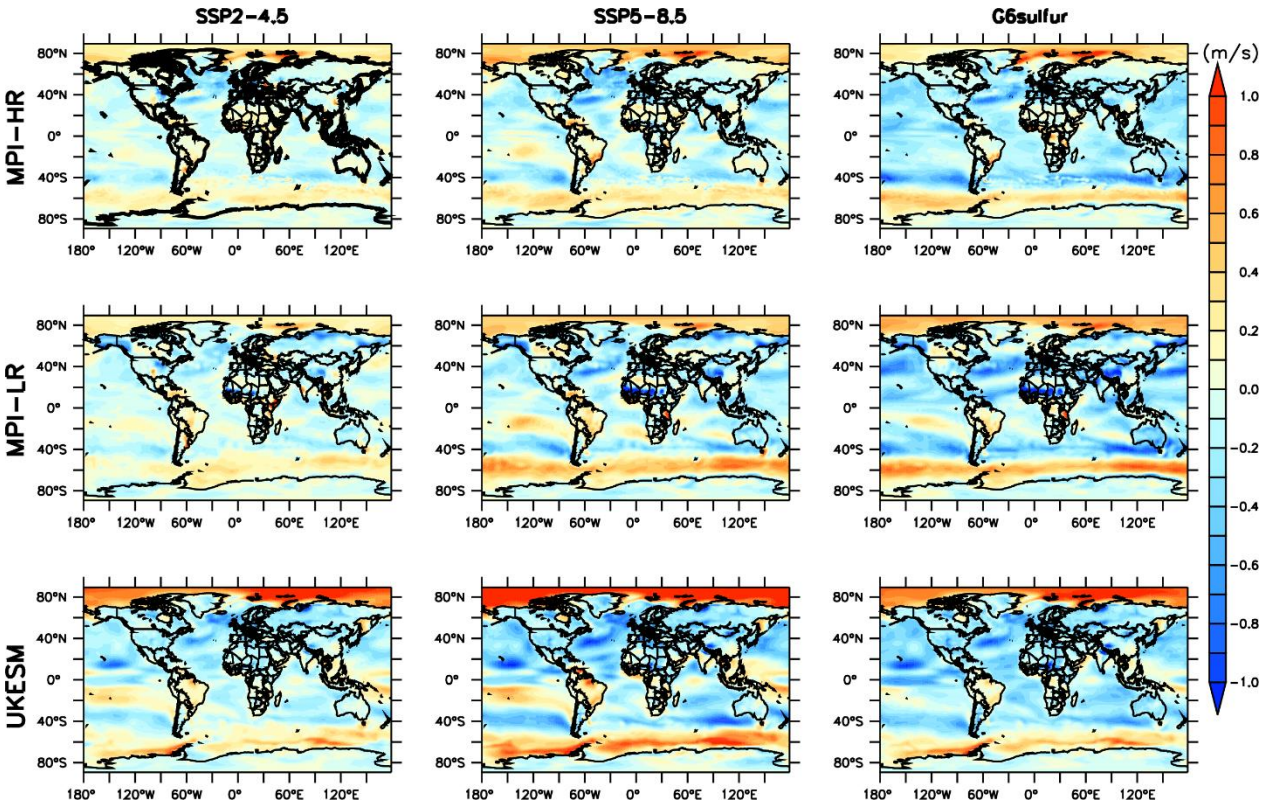

Figure 36 : Same as Figure.35, but in the far future (2070-2099)

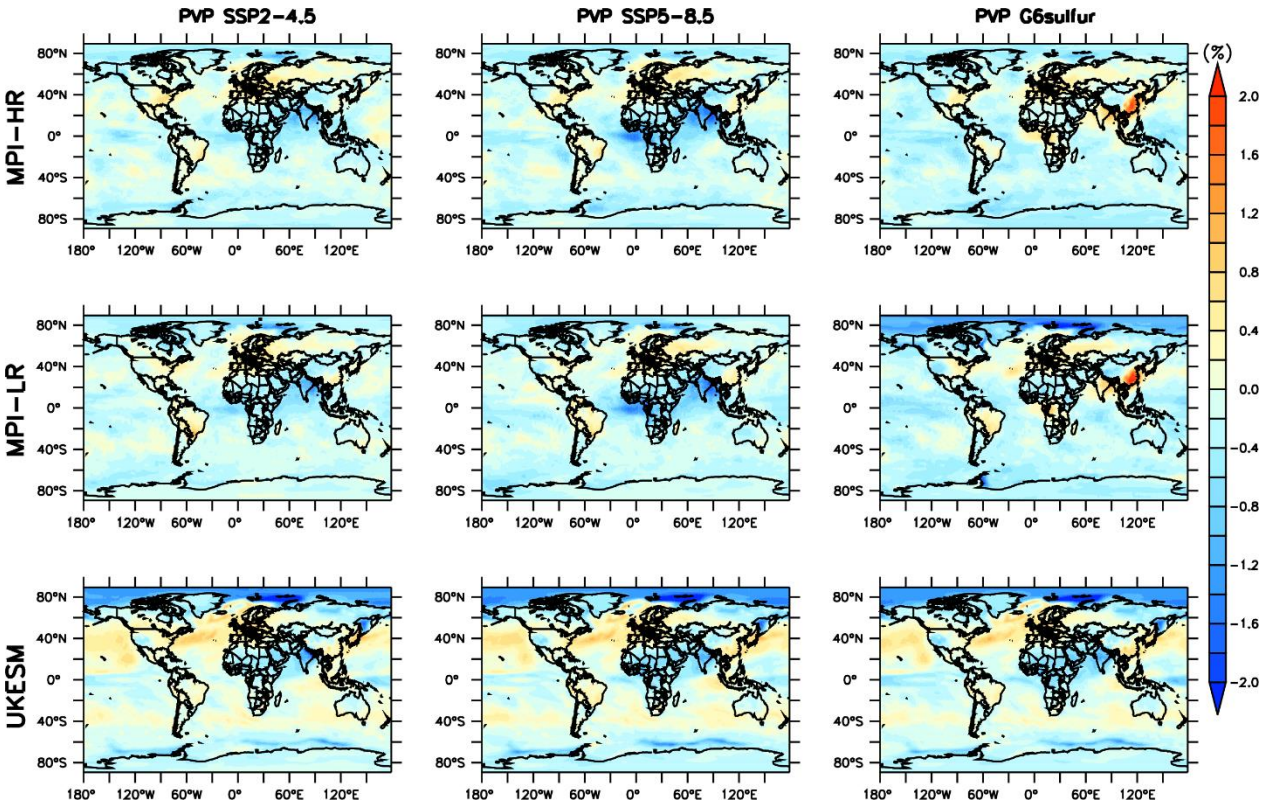

Figure 37 : Global mean of photovoltaic power potential (PVP) changes projected in the near future (2021-2050) of the three models (MPI-HR, MPI-LR, UKESM) under SSP2-4.5, SSP5-8.5, and G6sulfur scenarios.

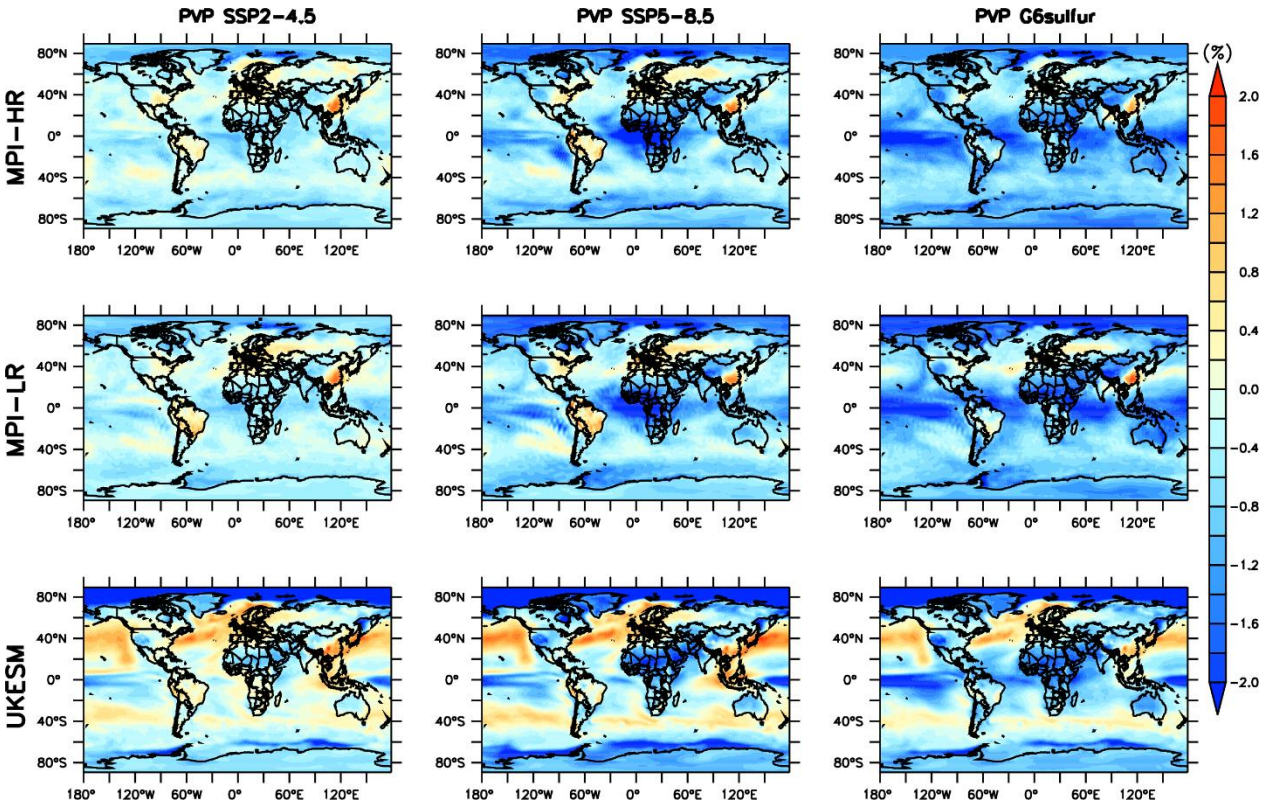

Figure 38 : Same as Figure.37, but in the far future (2070-2099)

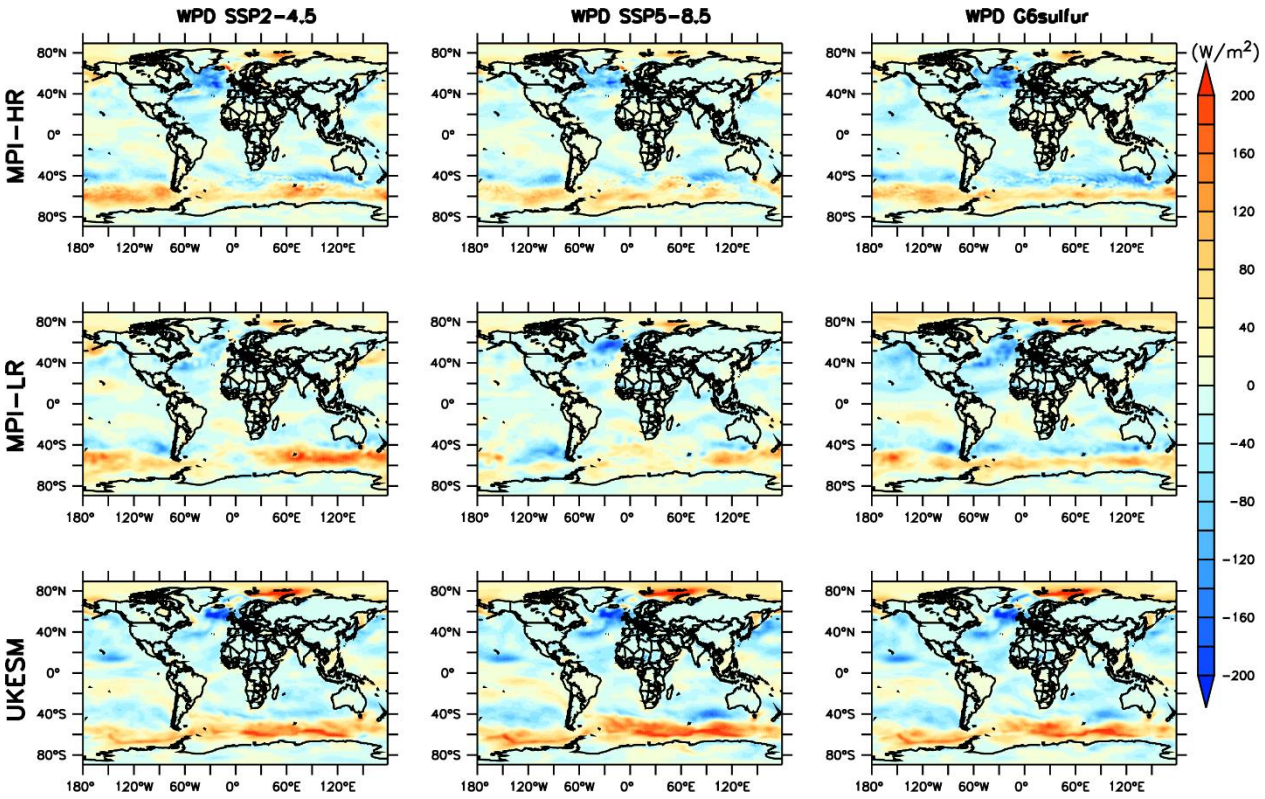

Figure 39 : Global mean of wind power density (WPD) changes projected in the near future (2021-2050) of the three models (MPI-HR, MPI-LR, UKESM) under SSP2-4.5, SSP5-8.5, and G6sulfur scenarios.

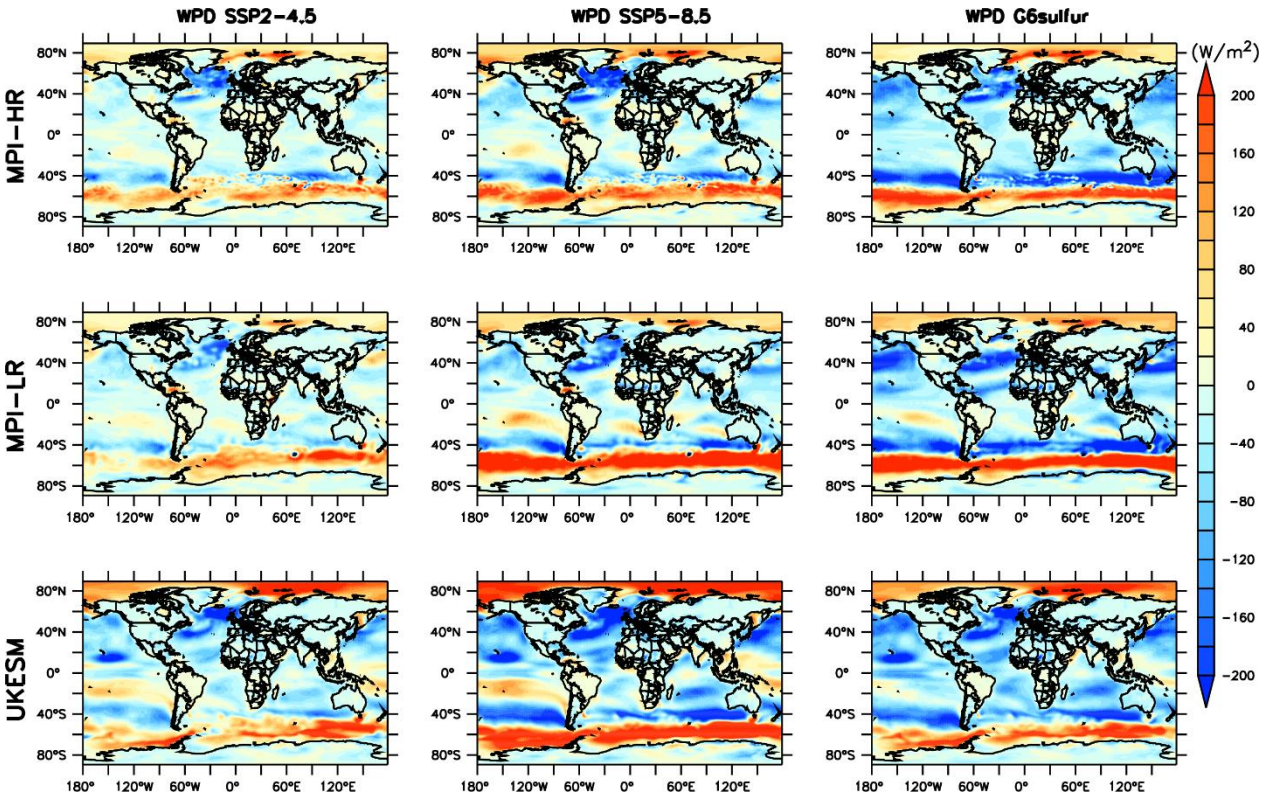

Figure 40 : Same as Figure.39, but in the far future (2070-2099)

Table of Contents